Journal of Medicinal Chemistry

pubs.acs.org/jmc

Article

Transferrin-Modified Carprofen Platinum(IV) Nanoparticles as Antimetastasis Agents with Tumor Targeting, Inflammation Inhibition, Epithelial−Mesenchymal Transition Suppression, and Immune Activation Properties

Ming Zhang, Yan Chen, Shuaiqi Feng, Yanqin He, Zhifang Liu, Ning Zhang, and Qingpeng Wang*

Cite This: J. Med. Chem. 2024, 67, 16416−16434

Read Online

ACCESS | Metrics & More | Article Recommendations | Supporting Information

ABSTRACT: The inflammatory microenvironment is a central driver of tumor metastasis, intimately associated with the promotion of epithelial−mesenchymal transition (EMT) and immune suppression. Here, transferrin-modified carprofen platinum(IV) nanoparticles Tf-NPs@CPF_2−Pt(IV) with promising antiproliferative and antimetastatic properties were developed, which activated by inhibiting inflammation, suppressing EMT, and activating immune responses besides causing DNA injury. The nanoparticles released the active ingredient CPF_2−Pt(IV) in a sustained manner and offered enhanced pharmacokinetic properties compared to free CPF_2−Pt(IV) in vivo. Additionally, they possessed satisfactory tumor targeting effects via the transferrin motif. Serious DNA damage was induced with the upregulation of γ-H2AX and P53, and the mitochondria-mediated apoptotic pathway Bcl-2/Bax/caspase3 was initiated. Inflammation was alleviated by inhibiting COX-2 and MMP9 and decreasing inflammatory cytokines TNF-α and IL-6. Subsequently, the EMT was reversed by inhibiting the Wnt/β-catenin pathway. Furthermore, the antitumor immunity was provoked by blocking the immune checkpoint PD-L1 and increasing $CD3^+$ and $CD8^+$ T lymphocytes in tumors.

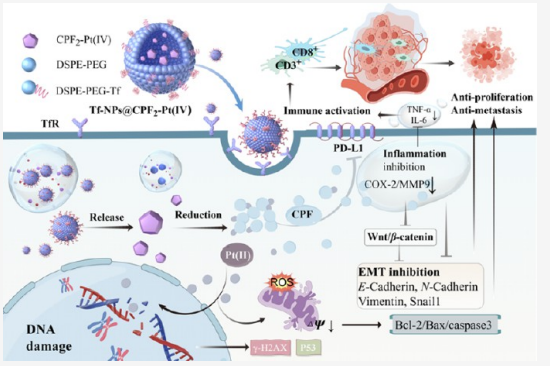

INTRODUCTION

Chemotherapy remains the cornerstone for the treatment of malignant tumors, providing long-term clinical benefits to patients afflicted with cancers. However, classical chemotherapeutics displayed rather limited effects on metastatic tumors, which are responsible for as much as 90% of cancer-associated mortality.[1,2] Curing or preventing metastasis of tumor cells during chemotherapy has attracted increasing attention in the antitumor field, and the development of novel antitumor agents with potent antiproliferative and antimetastatic properties appears to be the logical step forward in the design of new antitumor drugs.[3]

Platinum drugs, such as cisplatin (CDDP), carboplatin (CBP) and oxaliplatin (OXP) as the most successful metallic drugs, were widely applied in the treatment of various cancers. However, their therapeutic outcomes are seriously hindered by several limitations, including serious toxicity, bad tumor targeting properties, easily acquired drug resistance, and so on, which ultimately limit their therapeutic outcomes.[4] Additionally, they display rather limited efficacy toward metastatic tumors in the clinic. In this context, platinum(IV) prodrugs as nonconventional platinum-based anticancer agents that do not follow the original "structure−activity relationships" of platinum(II) drugs provide a fascinating scaffold to develop novel platinum drugs.[5−9] The octahedral coordination geometry of the platinum(IV) center allows for easy modification of the metal by introducing diverse functional axial ligands as desired. The construction of multifunctional platinum(IV) hybrids affords a meaningful approach for generating new drugs with promising antiproliferative and antimetastatic activities to defeat the drawbacks of the current platinum drugs.

Epithelial−mesenchymal transition (EMT) involving the phenotypic switch of epithelial cells to mesenchymal phenotype displays critical roles in promoting tumor metastasis,[10−13] while chronic inflammation as a hallmark of the tumor microenvironment (TME) is another promotor of metastasis.[14−16] Moreover, EMT and inflammation are of great potential in promoting each other wherein overexpressed COX-2 occurring in the inflammatory TME modulates the expression of EMT-related proteins (*E*-cadherin, *N*-cadherin,

Received: June 3, 2024
Revised: August 4, 2024
Accepted: August 30, 2024
Published: September 5, 2024

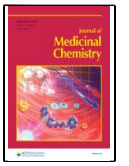

vimentin, and Snail1), which would conversely aggravate inflammatory responses in tumors. Notably, chronic inflammation and EMT conditions are also essential in inducing immunosuppression in TME,[17−20] which serves as another hallmark of cancers and displays dramatic stimulatory effects on the metastasis of tumor cells.[21,22] In accordance, inhibiting inflammation in the TME during chemotherapy might be a promising strategy to suppress EMT and reverse the immune suppressive effects in tumors, which would further elevate the potency of drugs against metastatic tumors.

The integration of nonsteroidal anti-inflammatory drugs (NSAIDs) into the platinum(IV) system was a promising way to modulate the inflammatory TME, and several platinum(IV) complexes with NSAID ligands, such as aspirin, indomethacin, ibuprofen, flurbiprofen, ketoprofen, niflumic acid, etc., have been designed, exerting promising antitumor activities in vitro and in vivo.[23−25] Our recent findings disclosed that these complexes exerted potent antimetastasis activities by suppressing the inflammatory TME besides damaging DNA.[26−28] However, the poor tumor targeting properties have become a major barrier to the further development of such NSAID platinum(IV) complexes. Encouraged by these observations, and as a continuation of our interest in developing novel platinum(IV) antitumor agents,[29−31] it was of great interest for us to further develop tumor-targeted agents as antiproliferative and antimetastatic drugs based on the NSAID platinum(IV) scaffold, and investigate their potential in suppressing EMT and activating immunity besides inhibiting inflammation.

Nanodrug delivery systems (NDDS) are effective tools for drug delivery and are of much potential in improving drug solubility and reducing side effects.[32−34] Nanoparticles (NPs) encapsulating platinum(IV) prodrugs have attracted abundant attention in the medicinal field, and some excellent work has been reported in the past decade.[35−39] Compared with the free platinum(IV) complex, the key features of platinum(IV) NDDS are as follows: (1) The nanocage prevents the platinum(IV) complex from the blood microenvironment during the transport, which would effectively decrease the reduction and inactivation of platinum(IV) conjugates by glutathione and metallothionein in blood and further reduce toxicity in vivo. (2) The enhanced permeability and retention (EPR) effects could improve the uptake of platinum(IV) agents in tumors to some extent. (3) The attractive pharmacokinetic (PK) properties and the slow-release behavior of nanodrugs in the tumors would be of much potential in improving the antitumor activities and decreasing toxicity. (4) More importantly, the modification of nanoparticles with tumor targeting motifs has shown considerable promise in bestowing nanoparticles with increased tumor targeting capabilities, thereby effectively enhancing the antitumor activity. Iron is an essential element for cell growth, which is highly desired during the unlimited proliferation of tumor cells. The transferrin receptor widely overexpressed on the surface of various tumor cells is a key protein mediating the cellular uptake of iron through the specific binding with protein transferrin (Tf).[40,41] Modification of nanoparticles with Tf is often selected for cancer therapy because of its promising tumor targeting effects.[42−44] Improving the tumor targeting effects of platinum(IV) conjugates with Tf-modified NDDS has not yet been studied; therefore, it deserves a careful investigation to further disclose its influence on the antitumor performance.

Carprofen (CPF), as an important NSAID, possesses remarkable COX-2 inhibitory effects; meanwhile, it is effective in suppressing the Wnt/β-catenin signaling,[45,46] which serves as a pivotal governor of the EMT process. Herein, CPF was incorporated into the platinum(IV) system, and CPF platinum(IV) complexes with a CDDP core were prepared (Figure 1). Encouragingly, it has been proven in the

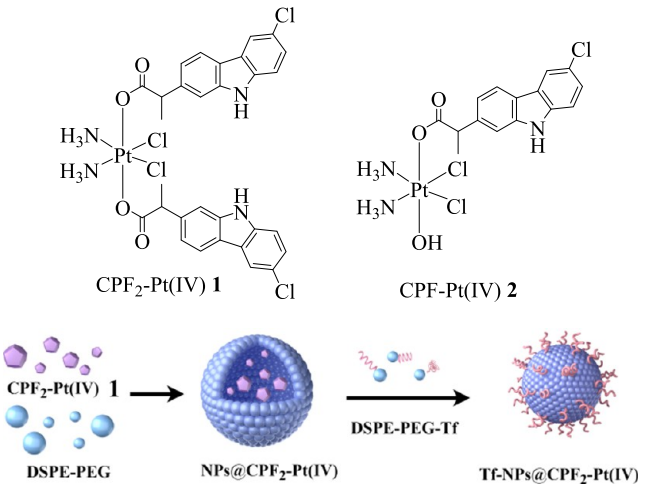

Figure 1. Structures of CPF_2−Pt(IV) **1**, CPF−Pt(IV) **2**, and nanoparticles NPs@CPF_2−Pt(IV) and Tf-NPs@CPF_2−Pt(IV).

literature[46] that complex CPF_2−Pt(IV) **1** exhibits promising antiproliferative and antimetastatic activities in vitro, but its antitumor performance in vivo still deserves to be detected. Then, mono CPF platinum(IV) complex CPF−Pt(IV) **2** was also prepared to detect the influence of ligands on the antitumor activities. After the primary antitumor screen in vitro, it was observed that the dual CPF platinum(IV) complex (CPF_2−Pt(IV) **1**) possessed superior antitumor performance to the mono ligand one (CPF−Pt(IV) **2**); thus, it was selected as a candidate in the following nanomedicine preparation. Amphiphilic DSPE-PEG with a structure similar to the cytomembrane possesses high biocompatibility in vivo. Thus, $DSPE\text{-}PEG_{2000}$ was selected as the carrier material to encapsulate CPF_2−Pt(IV) **1**, and nanoparticles NPs@CPF_2−Pt(IV) were prepared. Aiming to elevate the tumor targeting properties, Tf was modified on the surface of the nanoparticles, and Tf-NPs@CPF_2−Pt(IV) was generated. Subsequently, the antitumor activities for CPF platinum(IV) complexes **1** and **2** and nanoparticles NPs@CPF_2−Pt(IV) and Tf-NPs@CPF_2−Pt(IV) were evaluated both in vitro and in vivo. Then, the antimetastasis properties were further detected by in vitro and in vivo assays. Their likely mechanisms were also detected.

RESULTS AND DISCUSSION

Preparation and Characterization of CPF Platinum(IV) Complexes. The CPF platinum(IV) complexes were synthesized according to the procedures demonstrated in Scheme S1. Oxoplatin was synthesized starting from CDDP after oxidation by hydrogen peroxide. Then, the condensation of oxoplatin with 3.0 or 1.0 equiv of CPF in the presence of *N,N,N′,N′*-tetramethyl-O-(benzotriazol-1-yl)uronium tetrafluoroborate (TBTU) and *N,N,N*-triethylamine (TEA) afforded conjugates CPF_2−Pt(IV) **1**, and CPF−Pt(IV) **2** in yields of 30 and 24%, respectively. Their purity was confirmed by a high-performance liquid chromatography (HPLC) assay,

https://doi.org/10.1021/acs.jmedchem.4c01265
J. Med. Chem. 2024, 67, 16416−16434

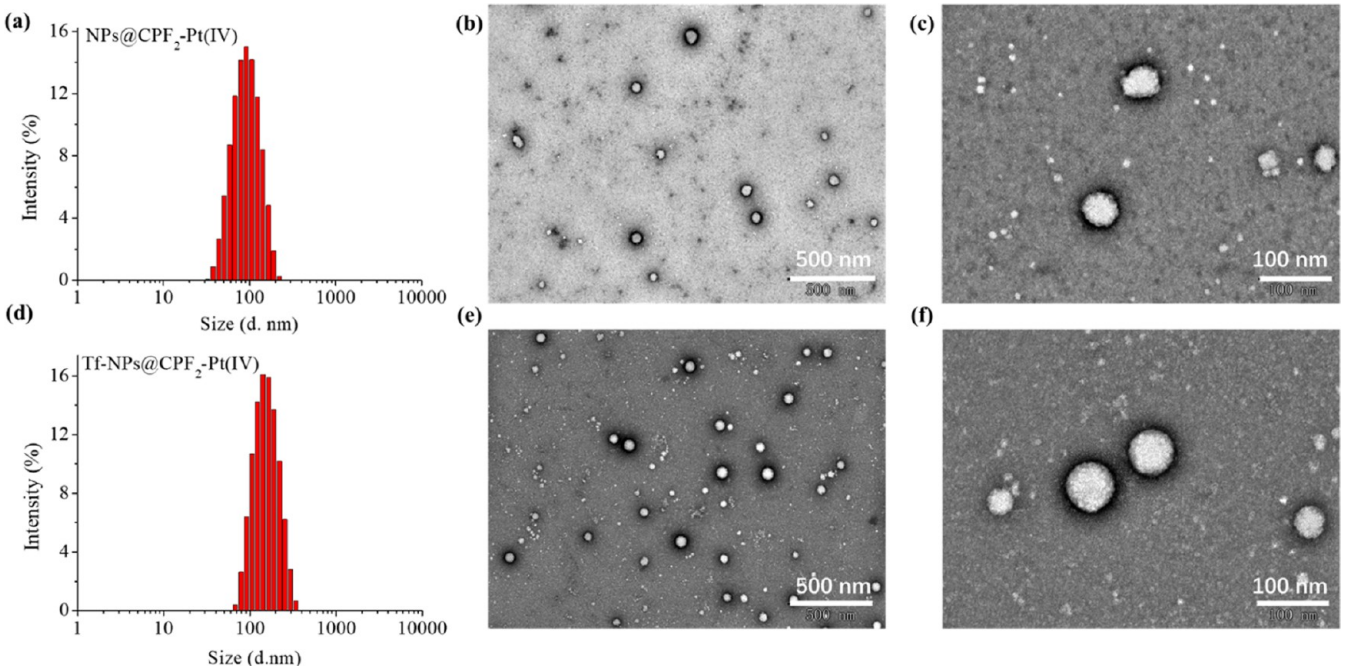

Figure 2. Particle size distribution determined by DLS and TEM: (a–c) NPs@CPF_2–Pt(IV) and (d–f) Tf-NPs@CPF_2–Pt(IV).

and both compounds were >95% pure. Their structures were confirmed by ^{1}H NMR, ^{13}C NMR, ESI-MS, and HRMS.

Preparation and Characterization of Nanoparticles. Before the preparation of nanoparticles, the antitumor activities for both CPF platinum(IV) complexes were evaluated by the MTT assay (see the Antiproliferative Activities In Vitro), and CPF_2–Pt(IV) **1** with dual CPF ligands exerted higher antitumor efficacy than the corresponding mono CFP hybrid (CPF–Pt(IV) **2**). Thus, nanoparticles NPs@CPF_2–Pt(IV) were prepared by encapsulating CPF_2–Pt(IV) **1** into DSPE-PEG_{2000}. The encapsulation efficiency was approximately 94%, as determined by atomic absorption spectrometry (AAS), which reflected that CPF_2–Pt(IV) **1** was almost entirely entrapped in the nanoparticles. Then, the Tf-modified nanoparticles Tf-NPs@CPF_2–Pt(IV) were obtained via the coincubation of DSPE-PEG_{2000}-Tf with NPs@CPF_2–Pt(IV). The particle size distributions for NPs@CPF_2–Pt(IV) (97.2 ± 1.4 nm, PDI = 0.11 ± 0.01, ζ = −15.24 ± 0.45 mV) and Tf-NPs@CPF_2–Pt(IV) (123.2 ± 3.5 nm, PDI = 0.32 ± 0.02, ζ = −17.03 ± 0.52) were determined using dynamic laser light scattering (DLS, Figure 2a,d). A slight increase of nanoparticle size for Tf-NPs@CPF_2–Pt(IV) was observed in contrast to NPs@CPF_2–Pt(IV), which was probably ascribed to the binding of DSPE-PEG_{2000}-Tf onto the surface of the nanoparticles. The binding ratio of Tf detected by the BCA kit was 89.4%, which would improve the tumor targeting properties of the nanoparticles. Moreover, the nanoparticles owning negative surface charges were reported to preferentially accumulate in tumor tissues rather than normal organs, which would further elevate the capacity for Tf-NPs@CPF_2–Pt(IV) targeting tumor tissues.[47] Subsequently, the morphology of nanoparticles was further characterized by transmission electron microscopy (TEM, Figure 2b,c,e,f). In line with the DLS results, NPs@CPF_2–Pt(IV) were uniform in size and well-rounded, while Tf-NPs@CPF_2–Pt(IV) also displayed a round shape with relatively larger particle sizes. Besides, due to the dehydration and wrinkling of the nanoparticles during the preparation of the TEM samples, both NPs@CPF_2–Pt(IV) and Tf-NPs@CPF_2–Pt(IV) showed smaller particle sizes in TEM images than those measured by DLS.

Subsequently, the stability of nanoparticles NPs@CPF_2–Pt(IV) and Tf-NPs@CPF_2–Pt(IV) was monitored for 21 days by detecting the particle size using DLS. The results in Figure S1 manifested that both nanoparticles exerted good stability in the aqueous state under 4 °C storage conditions, and the particle size fluctuated within a relatively acceptable range with increasing placement time.

Release Behavior of Complex 1 from Nanoparticles and Further Reduction in TME. The drug release behavior of nanoparticles displayed a dramatic influence on the antitumor performance in comparation with the injection of free drugs.[48−50] Thus, the releasing behavior of complex CPF_2–Pt(IV) **1** from nanoparticles NPs@CPF_2–Pt(IV) and Tf-NPs@CPF_2–Pt(IV) was evaluated to compare with the complex **1** injection (dissolved in media of PBS containing 5% DMF). The concentration of the active ingredient CPF_2–Pt(IV) **1** in the release solution was determined by measuring the Pt content using an AAS assay. Results in Figure S2 manifested that the complex **1** injection showed a burst release of up to 90% within the initial 4 h, exhibiting complete passive diffusion release behavior, while both nanoparticles displayed slower release rates. Complex **1** was released from NPs@CPF_2–Pt(IV) and Tf-NPs@CPF_2–Pt(IV) gradually for about 80% in 48 h. This long-term drug release behavior allowed the prolonged exposure of tumor cells to chemotherapeutics and further influenced the antitumor activities of the nanodrugs.

The platinum(IV) complexes as prodrugs of platinum(II) drugs are expected to remain stable in a biological medium and undergo a reduction in tumors. Herein, the stability of CPF_2–Pt(IV) **1** in RPMI1640 was detected by HPLC. The HPLC spectra in Figure S3 indicated that CPF_2–Pt(IV) **1** remained stable for at least 48 h in a biological medium. Then, it underwent an easy reduction in the reducing medium RPMI1640 with ascorbic acid (AsA, 1 mM, similar to that in

https://doi.org/10.1021/acs.jmedchem.4c01265
J. Med. Chem. 2024, 67, 16416−16434

Table 1. Antiproliferative Activities of CPF Platinum(IV) Complexes 1 and 2 and Nanoparticles NPs@CPF_2−Pt(IV) and Tf-NPs@CPF_2−Pt(IV) against Four Tumor Cell Lines with CPF, CDDP−CPF, CDDP, OXP, and STP as References[a]

complexes	A549	A549R	RF[b]	4T1	HepG2	LO2	SI[c]
1	1.69 ± 0.50	0.88 ± 0.11	0.52	0.91 ± 0.47	1.73 ± 0.60	6.45 ± 1.84	3.73
2	7.07 ± 1.07	1.86 ± 0.07	0.26	1.70 ± 0.41	2.05 ± 0.36	2.80 ± 0.14	1.37
CPF	32.23 ± 9.39	>50	ND[d]	>50	>50	24.23 ± 3.67	ND
CDDP−CPF[e]	6.94 ± 2.95	33.44 ± 1.16	4.82	7.16 ± 2.58	2.22 ± 0.23	3.87 ± 0.60	1.74
NPs@CPF_2−Pt(IV)	3.46 ± 1.66	1.02 ± 0.20	0.29	1.84 ± 0.18	2.39 ± 0.62	6.35 ± 1.05	2.66
Tf-NPs@CPF_2−Pt(IV)	3.19 ± 0.24	0.50 ± 0.08	0.16	0.83 ± 0.24	1.86 ± 0.16	8.53 ± 1.73	4.59
CDDP	5.30 ± 0.49	26.92 ± 4.32	5.08	3.41 ± 0.63	3.66 ± 1.00	2.81 ± 0.56	0.77
OXP	10.85 ± 1.46	14.31 ± 0.62	1.32	8.21 ± 1.25	11.95 ± 3.10	5.74 ± 0.12	0.48
STP	10.37 ± 0.71	14.65 ± 0.69	1.41	10.30 ± 3.43	8.18 ± 3.45	5.71 ± 0.42	0.70

[a]Cells were treated with drugs for 48 h, and the half maximal inhibitory concentration (IC_{50}, μM) was given based on three parallel experiments. [b]RF: resistant factor, RF = IC_{50}(A549R)/IC_{50}(A549). [c]SI: selective index, SI = IC_{50}(LO2)/IC_{50}(HepG2). [d]ND: not tested or not calculated. [e]CDDP−CPF: a mixture of CDDP and CPF with a molar ratio of 1:2.

TME) so that the peak of CPF_2−Pt(IV) **1** shrunk gradually, accompanied by the increase of the CPF peak (Figure S5). Subsequently, guanosine-5′-monophosphate (5′-GMP) was added as a model of DNA base. The emergence of a platinate GMP peak (verified by the MS spectrum) evidenced the potent DNA binding properties of CPF_2−Pt(IV) **1** (Figure S6), attributing to the platinum(II) counterpart released after the reduction.

Therefore, it was reasonable to conclude that the active ingredient CPF_2−Pt(IV) **1** could be released from nanoparticles Tf-NPs@CPF_2−Pt(IV) and NPs@CPF_2−Pt(IV) in a sustained release manner, which displayed satisfactory stability in a biological medium. Then, it underwent an easy reduction to platinum(II) form in reducing TME and further bound with DNA in tumors. These promising release behaviors and reduction properties were of great potential in improving the antitumor activities of the title nanoparticles based on CPF platinum(IV) hybrids. Subsequently, the in vitro and in vivo antitumor activities were evaluated in the following experiments.

Antiproliferative Activities In Vitro. The antiproliferative activities of CPF platinum(IV) complexes **1** and **2** and nanoparticles NPs@CPF_2−Pt(IV) and Tf-NPs@CPF_2−Pt(IV) were evaluated in vitro by the MTT assay against four tumor cell lines, including human lung cancer (A549), CDDP-resistant human lung cancer (A549R), murine breast cancer (4T1), and human liver cancer (HepG2), and one normal human liver cell line (LO2), with platinum(II) drugs CDDP and OXP and platinum(IV) drug STP as references. The ligand CPF and the mixture of CDDP and CPF (CDDP−CPF) with a molar ratio of 1:2 were also evaluated.

The results in Table 1 revealed that both CPF platinum(IV) complexes **1** and **2** possessed effective antitumor performance with IC_{50} values lower than 7.07 μM against all tested tumor cells. Furthermore, dual CPF platinum(IV) complex **1** possessing a higher uptake level in whole tumor cells than the mono CPF conjugate CPF−Pt(IV) **2** ($P < 0.01$, Figure S7a) led to relatively superior antitumor potency. It displayed low $IC_{50} \leq 1.73$ μM against all tested tumor cell lines, which mainly coincided with those disclosed in the literature.[46] Notably, the ligand CPF exerted negligible antitumor performance ($IC_{50} \geq 32.23$ μM) in contrast to the CPF platinum(IV) conjugates against all of the tumor cell lines, the trend of which was also observed in the literature.[46] Meanwhile, the mixture CDDP−CPF displayed antitumor potency similar to that of CDDP. These facts disclosed that the conjugation of CPF with a platinum system was a necessary step to improve the antitumor efficacy. Regarding the better antitumor activities of CPF_2−Pt(IV) **1** than those of CPF−Pt(IV) **2**, complex **1** was selected as the active ingredient for the preparation of nanoparticles. Subsequently, NPs@CPF_2−Pt(IV) and Tf-NPs@CPF_2−Pt(IV) were prepared. It was observed that Tf-NPs@CPF_2−Pt(IV) with Tf modification exhibited higher activities than NPs@CPF_2−Pt(IV) and free complex **1**, which was also significantly more potent than CDDP. These facts were probably owing to the higher uptake of Tf-NPs@CPF_2−Pt(IV) in tumor cells than free complex **1** ($P < 0.001$) and NPs@CPF_2−Pt(IV) ($P < 0.05$, Figure S7a).

The resistance of tumor cells to platinum drugs has always been a clinical conundrum during cancer treatment. To evaluate the potency of the tested agents in overcoming drug resistance of CDDP, the resistant factor (RF) as a ratio of the IC_{50} value for A549R to that of A549 was calculated. Both CPF platinum(IV) complexes **1** and **2** and nanoparticles NPs@CPF_2−Pt(IV) and Tf-NPs@CPF_2−Pt(IV) exhibited fascinating properties in overcoming the drug resistance with RF values lower than 0.52, which were over 9-fold lower than the value for CDDP (5.08); meanwhile, the mixture CDDP−CPF resulted in rather negligible impacts on the drug resistance with a high RF of 4.82. In particular, nanoparticles Tf-NPs@CPF_2−Pt(IV) possessed the most effective RF of 0.16, even lower than nanoparticles NPs@CPF_2−Pt(IV) (RF = 0.29) and free complex **1** (RF = 0.52). After that, the selective index (SI) as a ratio of the IC_{50} value for LO2 to that of HepG2 was calculated with the aim of assessing the toxicity in vitro primarily. It was realized that dual CPF platinum(IV) complexes CPF_2−Pt(IV) **1** displayed a decreased toxic performance (SI = 3.73) in contrast to CDDP (SI = 0.77) and the mixture CDDP−CPF (SI = 1.74); meanwhile, mono CPF platinum(IV) complex CPF−Pt(IV) **2** exerted a rather lower SI of 1.37. The nanoparticles also exerted promising properties in decreasing toxicity, especially Tf-NPs@CPF_2−Pt(IV) displayed the highest SI of 4.59, which was superior to that of NPs@CPF_2−Pt(IV) (SI = 2.66).

In accordance, the CPF platinum(IV) complexes, especially CPF_2−Pt(IV) **1**, represented a promising scaffold for anticancer drug exploration. Tf-modified nanoparticles Tf-NPs@CPF_2−Pt(IV) based on complex **1** further improved the antitumor efficacy in vitro and exhibited potent antitumor properties against all of the tested tumor cell lines. Moreover, Tf-NPs@CPF_2−Pt(IV) showed great potential in overcoming the drug resistance of CDDP and decreasing toxicity, which

https://doi.org/10.1021/acs.jmedchem.4c01265
J. Med. Chem. 2024, 67, 16416−16434

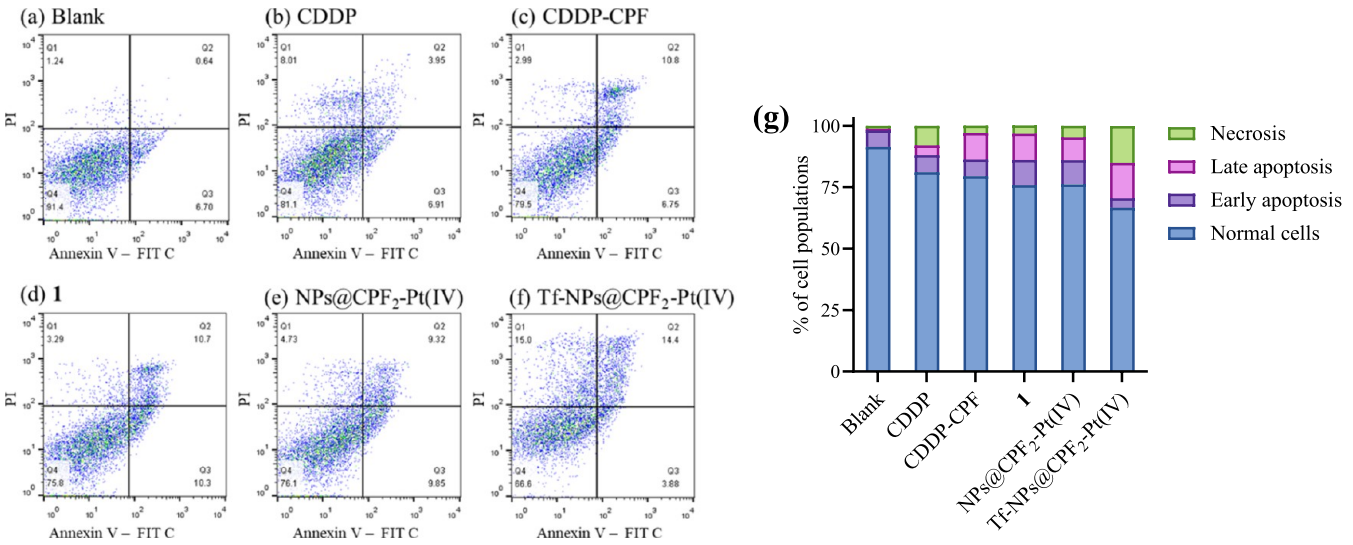

Figure 3. Quantification of apoptosis using a V-FITC/PI annexin staining assay. The 4T1 tumor cells were incubated with and without platinum complexes for 24 h at 37 °C. (a) Blank, (b) CDDP (5 μM), (c) CDDP−CPF (5 μM/10 μM), (d) compound **1** (5 μM), (e) NPs@CPF_2−Pt(IV) (5 μM), and (f) Tf-NPs@CPF_2−Pt(IV) (5 μM). (g) The stacking columns.

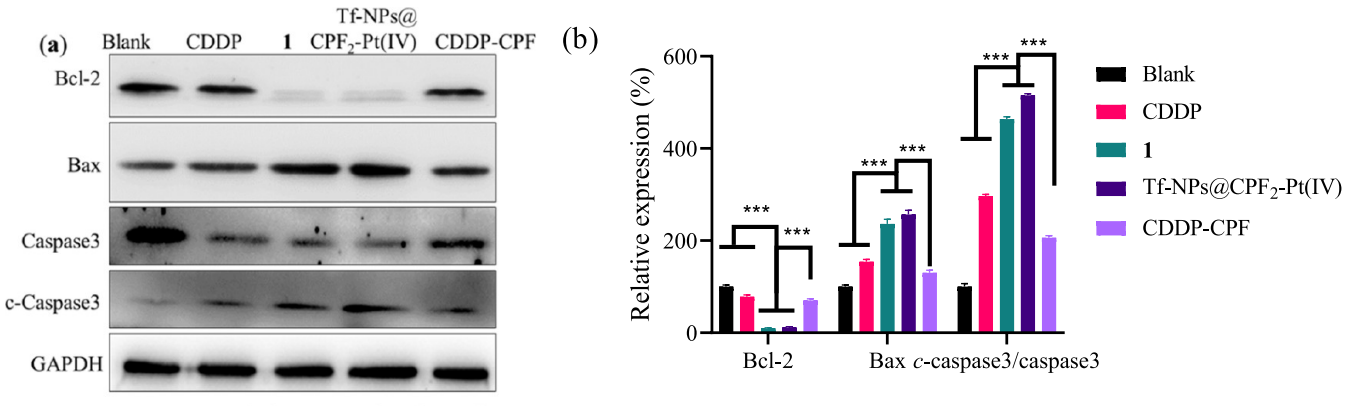

Figure 4. Western blot analysis of Bcl-2, Bax, caspase3, and *c*-caspase3 in 4T1 cells treated with and without CDDP (5 μM), complex **1** (5 μM), Tf-NPs@CPF_2−Pt(IV) (5 μM), and CDDP−CPF (5 μM/10 μM) for 24 h at 37 °C. (a) Blots. (b) Relative gray intensity analysis. Relative gray intensity = (gray intensity of indicated protein)/(gray intensity of GAPDH). ***$P < 0.001$.

was more effective than NPs@CPF_2−Pt(IV) and free complex **1**. These facts were probably related to the elevated tumor targeting properties due to Tf modification.

Induction of Mitochondria-Mediated Apoptosis. Apoptosis is one of the most critical mechanisms of programmed cell death, which is involved in the mechanism induced by platinum drugs. Herein, apoptosis-inducing properties were detected by flow cytometry using an Annexin V-FITC/propidium iodide (PI) double staining assay. The results in Figure 3 disclosed that CPF_2−Pt(IV) **1** was potent in inducing the apoptosis of tumor cells, which was similar to that of CDDP and CDDP−CPF. Then, nanoparticles NPs@CPF_2−Pt(IV) and Tf-NPs@CPF_2−Pt(IV) also displayed great potency in causing apoptosis. This trend was mainly in accordance with the antitumor efficacy in vitro.

Mitochondria have been recognized as crucial cellular organelles for apoptosis induction. Mitochondrial damage accompanied by the collapse of mitochondrial membrane potential ($\Delta\Psi_m$) and the production of reactive oxygen species (ROS) are common features of apoptosis. The JC-1 staining assay (Figure S8) reflected that free complex **1** and nanoparticles NPs@CPF_2−Pt(IV) and Tf-NPs@CPF_2−Pt(IV) induced a serious collapse of $\Delta\Psi_m$ of tumor cells, which indicated the mitochondria injury caused by these agents. Subsequently, ROS generation stained by 2′,7′-dichlorofluorescein diacetate (DCFH-DA) in free complex **1** and nanoparticles NPs@CPF_2−Pt(IV)- and Tf-NPs@CPF_2−Pt(IV)-treated groups also increased remarkably in comparison with the blank group (Figure S9). These facts manifested that CPF platinum(IV) complexes and their nanoparticles promoted the apoptosis of tumor cells effectively by causing serious mitochondria damage.

Bcl-2 signaling is pivotal in governing the mitochondria-mediated intrinsic apoptosis pathway. Thereby, proteins Bcl-2, Bax, caspase3, and *c*-caspase3 associated with Bcl-2 signaling were analyzed using the western blot assay. The blots in Figure 4 revealed that the antiapoptotic protein Bcl-2 in tumor cells was inhibited by complex **1** and nanoparticles Tf-NPs@CPF_2−Pt(IV), which was superior to CDDP and CDDP−CPF ($P < 0.001$). Then, the expression of the pro-apoptotic protein Bax was promoted by complex **1** and Tf-NPs@CPF_2−Pt(IV) in comparison with the blank group ($P < 0.001$). Subsequently, the ratios for apoptosis executive proteins *c*-caspase3/caspase3 were also remarkably elevated in complex **1** and Tf-NPs@

https://doi.org/10.1021/acs.jmedchem.4c01265
J. Med. Chem. 2024, 67, 16416−16434

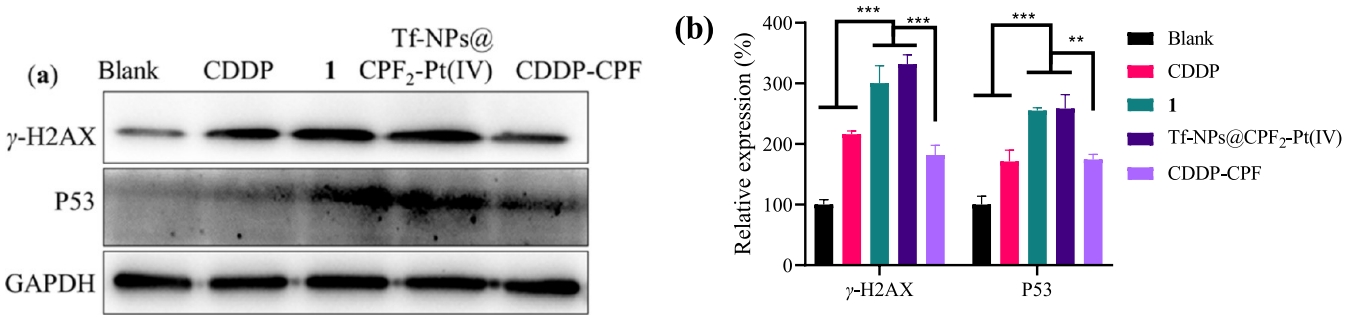

Figure 5. Western blot analysis of γ-H2AX and P53 in 4T1 cells treated with and without CDDP (5 μM), complex **1** (5 μM), Tf-NPs@CPF_2−Pt(IV) (5 μM), and CDDP−CPF (5 μM/10 μM) for 24 h at 37 °C. (a) Blots. (b) Relative gray intensity analysis. $^{**}P < 0.01$ and $^{***}P < 0.001$.

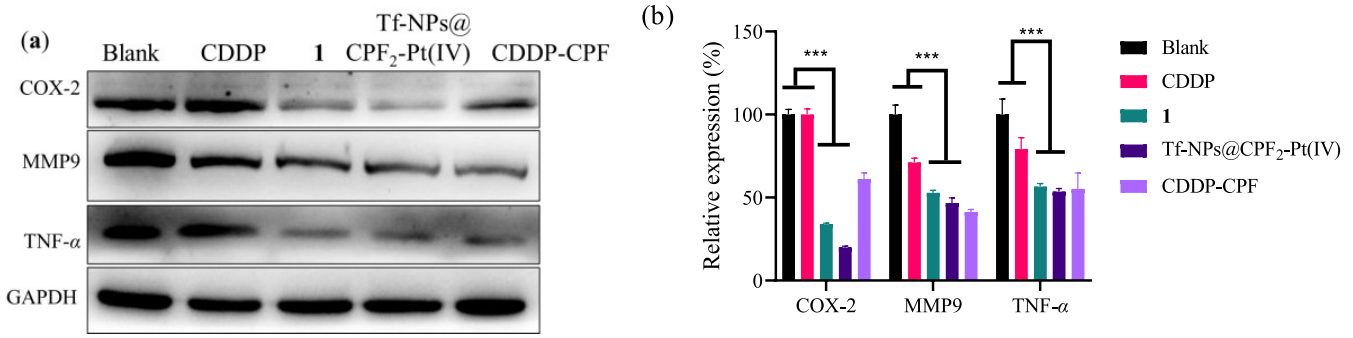

Figure 6. Western blot analysis of COX-2, MMP9, and TNF-α in 4T1 cells treated with and without CDDP (5 μM), complex **1** (5 μM), Tf-NPs@CPF_2−Pt(IV) (5 μM), and CDDP−CPF (5 μM/10 μM) for 24 h at 37 °C. (a) Blots. (b) Relative gray intensity analysis. $^{***}P < 0.001$.

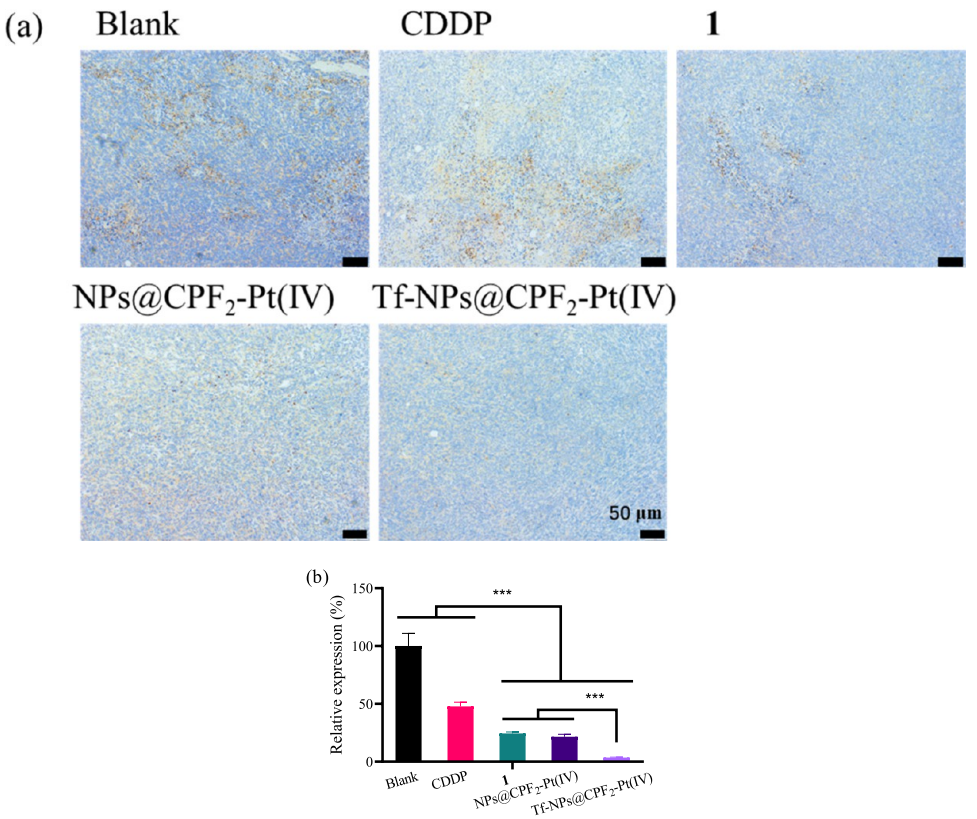

Figure 7. Expression of COX-2 in the tumor tissues of the blank, CDDP, complex **1**, and nanoparticles NPs@CPF_2−Pt(IV) and Tf-NPs@CPF_2−Pt(IV) groups in the antitumor growth assay in vivo was tested by immunohistochemistry. (a) Representative micrographs. (b) Quantified data of COX-2. $^{***}P < 0.001$.

https://doi.org/10.1021/acs.jmedchem.4c01265
J. Med. Chem. 2024, 67, 16416−16434

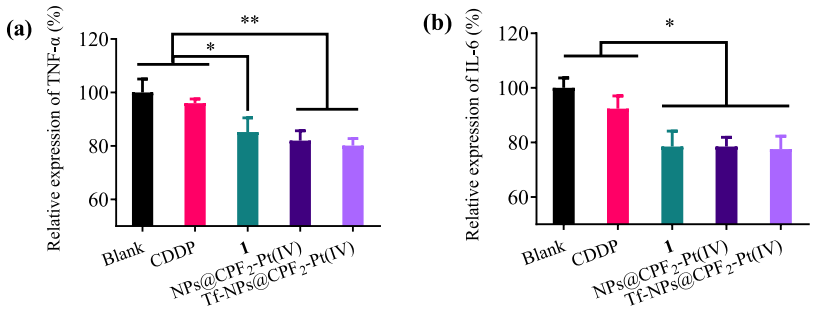

Figure 8. Secretion of TNF-α and IL-6 in tumor tissues tested by the ELISA assay. Tissues were obtained from the antitumor growth assay in vivo. Data were given based on three parallel experiments. (a) Quantified data of TNF-α. (b) Quantified data of IL-6. *P < 0.05 and **P < 0.01.

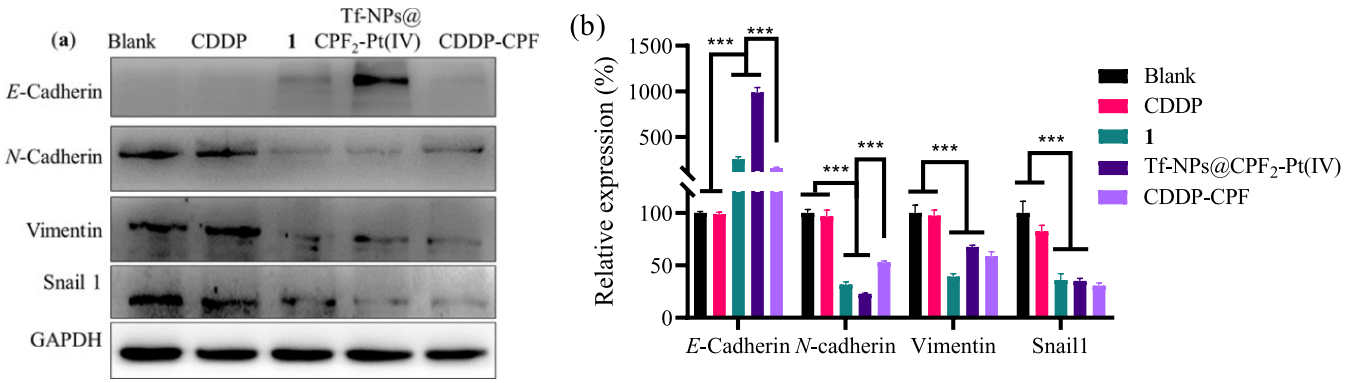

Figure 9. Western blot analysis of *E*-cadherin, *N*-cadherin, vimentin, and Snail1 in 4T1 cells treated with and without CDDP (5 μM), complex **1** (5 μM), Tf-NPs@CPF_2−Pt(IV) (5 μM), and CDDP−CPF (5 μM/10 μM) for 24 h at 37 °C. (a) Blots. (b) Relative gray intensity analysis. ***P < 0.001.

CPF_2−Pt(IV) treated groups, which were even higher than that of CDDP and CDDP−CPF (P < 0.001).

In accordance, CPF platinum(IV) complex **1** was effective in inducing mitochondria-mediated apoptosis through the Bcl-2/Bax/caspase3 pathway; meanwhile, nanoparticles Tf-NPs@CPF_2−Pt(IV) exhibited similar characteristics, mainly attributing to the embedment of complex **1**.

Causing DNA Damage. DNA damage was the crucial mechanism for platinum drugs to induce the apoptosis of tumor cells. The distribution of platinum drugs in the nucleus is critical for platinum drugs. Herein, the subdistribution of CPF platinum(IV) conjugates and the nanoparticles in tumor cells was detected by the AAS assay, and the DNA damage properties were evaluated by the western blot assay.

The cellular subdistribution results in Figure S7b revealed that the accumulation of complex **1** and nanoparticles NPs@CPF_2−Pt(IV) and Tf-NPs@CPF_2−Pt(IV) in the nucleus was higher than that of CDDP and the mixture CDDP−CPF (P < 0.001). Moreover, Tf-NPs@CPF_2−Pt(IV) led to more accumulation in DNA than free complex **1** and nanoparticles NPs@CPF_2−Pt(IV), which was mainly in tune with the uptake in whole cells (Figure S7a). These facts were probably ascribed to the better tumor targeting properties induced by the Tf motif.

Regarding the effective binding properties of CPF_2−Pt(IV) **1** revealed by HPLC (see the Release Behavior of Complex 1 from Nanoparticles and Further Reduction in TME), the DNA injury properties were subsequently testified by western blotting. The protein γ-H2AX is regarded as a sensitive indicator of DNA injury, while the tumor suppressor P53 is another central player in the cellular DNA damage response. It was realized in Figure 5 that the secretions of γ-H2AX and P53 were elevated significantly by complex **1** and nanoparticles Tf-NPs@CPF_2−Pt(IV) in contrast to the blank group (P < 0.001), which were even higher than CDDP and the mixture CDDP−CPF (P < 0.01).

In total, the antitumor agents including complex **1** and nanoparticles Tf-NPs@CPF_2−Pt(IV) were potent in causing serious DNA damage and further increased the expression of γ-H2AX and P53 in tumor cells.

Suppressing Inflammation. Chronic inflammatory TME, as one of the main hallmarks of malignant tumors, increases the expression of COX-2, which is potent in promoting the secretion of MMP9. COX-2 and MMP9 will in turn promote inflammation and elevate the expression of proinflammatory cytokines such as tumor necrosis factor (TNF)-α and interleukin (IL)-6, which serve as important modulators of proliferation, survival, metastasis, and immune escape of tumor cells. Herein, the expression of COX-2 was detected by western blotting and immunohistochemistry, and the expression of MMP9 was also tested by western blotting. The ELISA assay was subsequently applied to detect the secretion of inflammatory cytokines TNF-α and IL-6 in tumor tissues, and TNF-α in 4T1 tumor cells was also measured by western blotting.

The results in Figures 6 and 7 disclosed that the key inflammatory protein COX-2 was obviously inhibited by potent nanoparticles Tf-NPs@CPF_2−Pt(IV) both in vitro and in vivo in comparison with the blank group and CDDP (P < 0.001), which was similar or even superior to free complex **1**. Then, the expression of MMP9 was also remarkably inhibited, which was lower than the blank and CDDP groups (P < 0.001). Following that, the secretion of inflammatory cytokines TNF-α (P < 0.01) and IL-6 (P < 0.05) were suppressed to low

https://doi.org/10.1021/acs.jmedchem.4c01265
J. Med. Chem. 2024, 67, 16416−16434

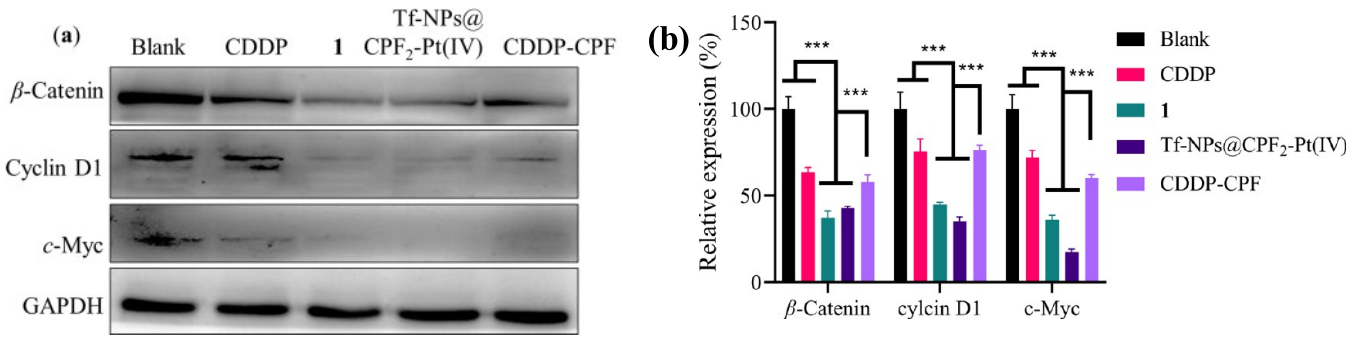

Figure 10. Western blot analysis of β-catenin, cyclin D1, and c-Myc in 4T1 cells treated with and without CDDP (5 μM), complex **1** (5 μM), Tf-NPs@CPF_2−Pt(IV) (5 μM), and CDDP−CPF (5 μM/10 μM) for 24 h at 37 °C. (a) Blots. (b) Relative gray intensity analysis. ***P < 0.001.

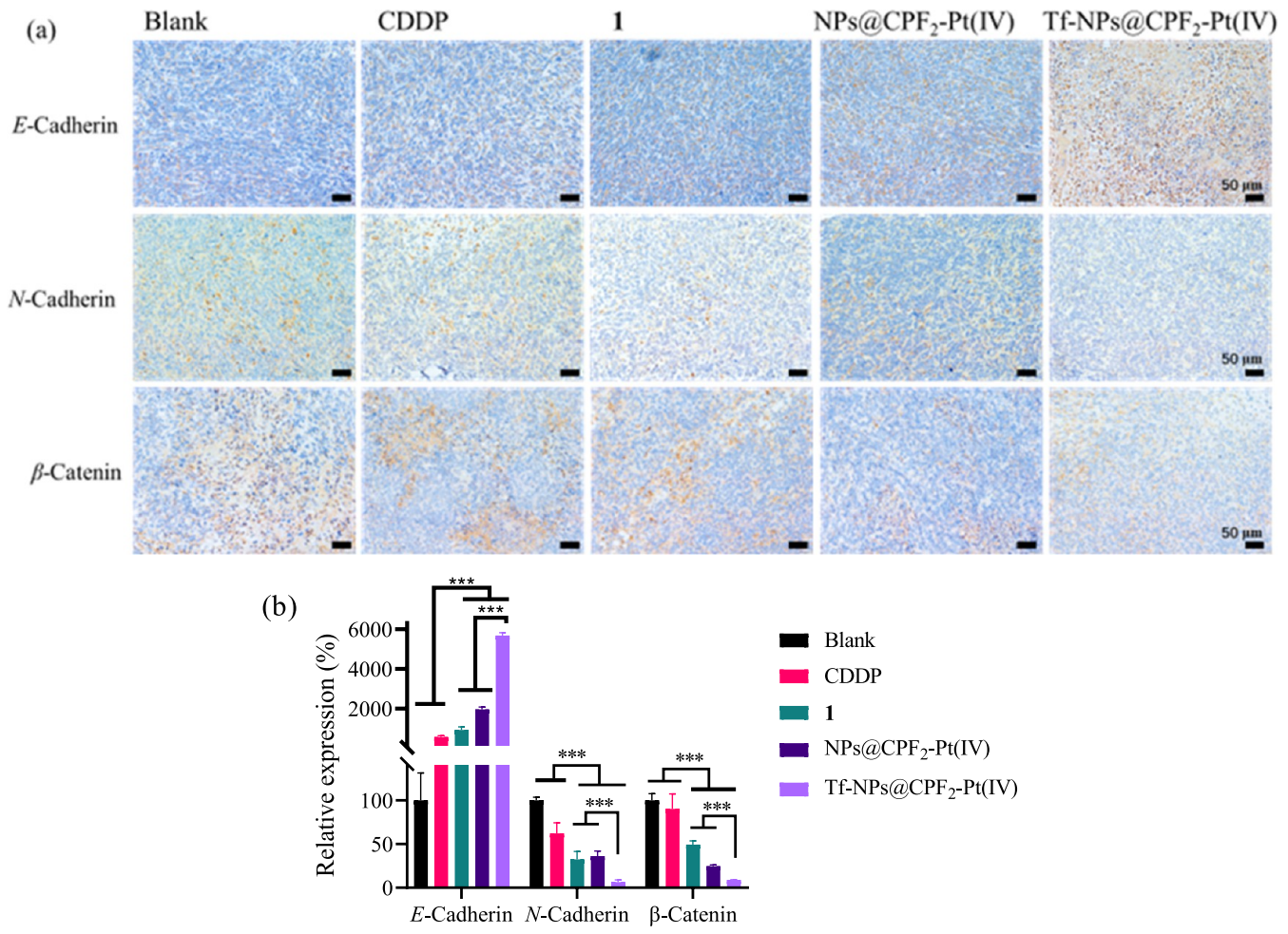

Figure 11. Expression of E-cadherin, N-cadherin, and β-catenin in tumor tissues of the blank, CDDP, complex **1**, and nanoparticles NPs@CPF_2−Pt(IV) and Tf-NPs@CPF_2−Pt(IV) groups in the antitumor growth assay in vivo was tested by immunohistochemistry. (a) Representative micrographs. (b) Quantified data. ***P < 0.001.

levels by Tf-NPs@CPF_2−Pt(IV) in tumor tissues compared with the blank and CDDP groups (Figure 8), which was mainly ascribed to the inflammation inhibitory competence from the CPF ligand. Then, the downregulation of TNF-α was also verified by the western blot assay in Tf-NPs@CPF_2−Pt(IV)-treated tumor cells (Figure 6).

Accordingly, nanomedicine Tf-NPs@CPF_2−Pt(IV) exerted great potency in suppressing inflammatory responses in TME by inhibiting the expression of COX-2 and MMP9 simultaneously and further suppressing TNF-α and IL-6 secretion.

Inhibiting EMT through the Wnt/β-Catenin Pathway. The EMT is a critical step in tumor invasion and metastasis and is of great potential in expediting the immune suppression in TME.[51] Wnt/β-catenin signaling serves as a versatile modulator of EMT, and the canonical Wnt/β-catenin/EMT axis has been implicated in augmenting the metastasis of diverse tumors. Moreover, overexpression of COX-2 showed an important crosstalk with the Wnt/β-catenin pathway in

https://doi.org/10.1021/acs.jmedchem.4c01265
J. Med. Chem. 2024, 67, 16416−16434

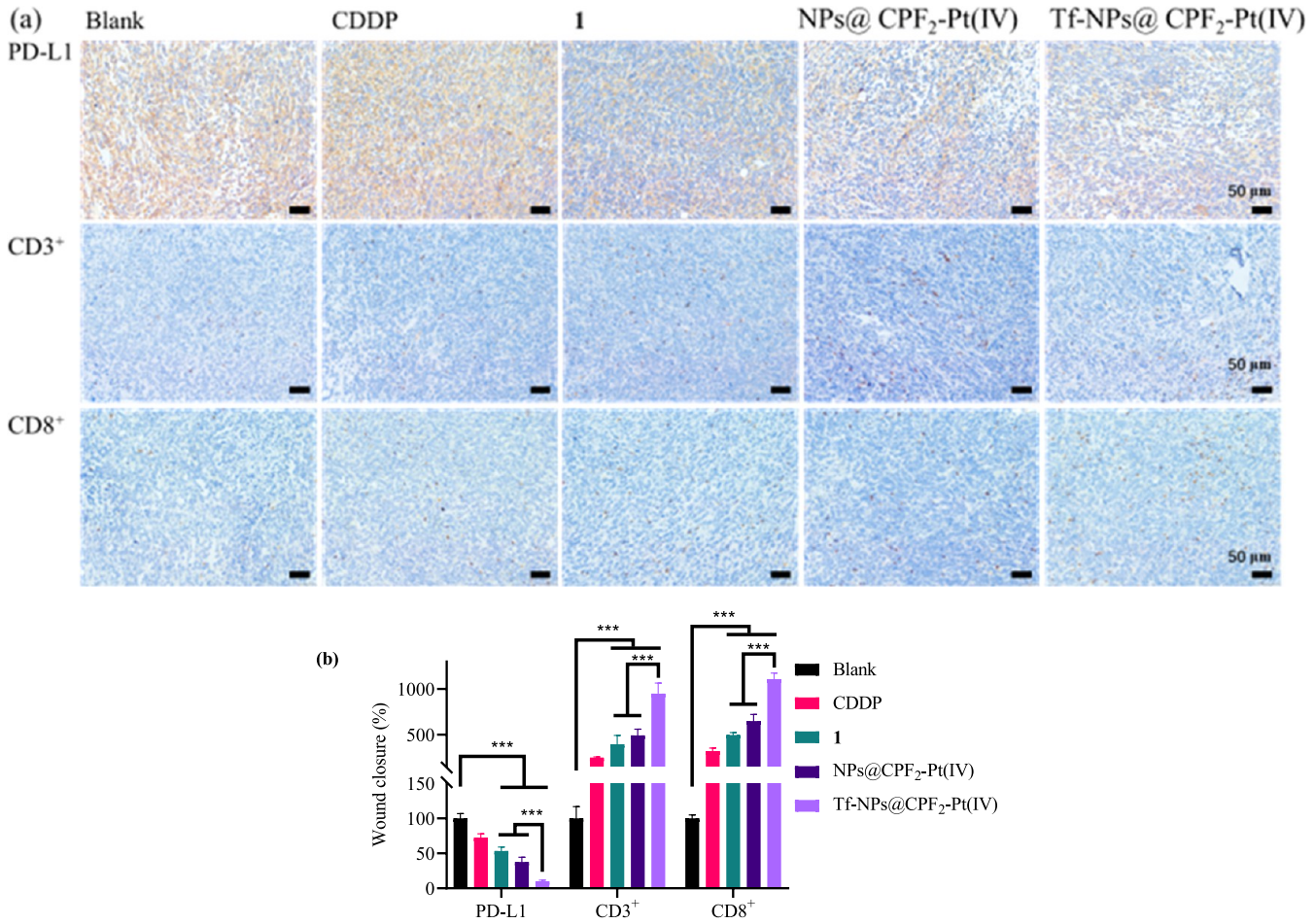

Figure 12. Immunohistochemical staining of PD-L1 expression, and TILs in tumor tissues of the blank, CDDP, complex **1**, and nanoparticles NPs@CPF_2−Pt(IV) and Tf-NPs@CPF_2−Pt(IV) groups in the antitumor growth assay in vivo. (a) Representative micrographs. (b) Quantified data of PD-L1, $CD3^+$, and $CD8^+$ TILs. $^{**}P < 0.01$ and $^{***}P < 0.001$.

TME in stimulating the proliferation and metastasis of tumor cells.[52,53] Herein, the expression of typical EMT markers *E*-cadherin, *N*-cadherin, vimentin, and Snail1 was detected by the western blot and immunohistochemistry assays to determine if the EMT process was suppressed by CPF_2−Pt(IV) **1** and the nanoparticles. Then, the Wnt/*β*-catenin pathway proteins *β*-catenin, cyclin D1, and *c*-Myc in 4T1 cells were also evaluated.

The blots in Figure 9 disclosed that *E*-cadherin was upregulated by complex **1** and nanomedicine Tf-NPs@CPF_2−Pt(IV) in contrast to the blank and CDDP groups ($P < 0.001$), while the downregulation of *N*-cadherin, vimentin, and Snail1 was also observed ($P < 0.001$). These facts demonstrated the reversion of the EMT phenotype in complex **1** and nanoparticles Tf-NPs@CPF_2−Pt(IV)-treated tumor cells. Then, this phenomenon was further verified by the immunohistochemical staining results in tumors in vivo (Figure 11) that the improvement of *E*-cadherin expression ($P < 0.001$) and the downregulation of *N*-cadherin ($P < 0.001$) were observed in complex **1** and nanoparticles NPs@CPF_2−Pt(IV) and Tf-NPs@CPF_2−Pt(IV)-treated tumor tissues in comparison with the blank and CDDP groups. It was noticed that Tf-NPs@CPF_2−Pt(IV) exerted even superior EMT reversing competence to free compound **1** and nanoparticles NPs@CPF_2−Pt(IV), which was probably ascribed to its enhanced tumor targeting effects.

It was realized that the EMT-suppressing efficacy for CPF_2−Pt(IV)-based agents was related to the suppression of the Wnt/*β*-catenin pathway. Results in Figure 10 demonstrated that *β*-catenin, cyclin D1, and *c*-Myc were downregulated simultaneously by complex **1** and nanoparticles Tf-NPs@CPF_2−Pt(IV) in 4T1 cells compared with the blank, CDDP, and CDDP−CPF groups ($P < 0.001$). This trend was further evidenced by the immunohistochemistry results in Figure 11 that the accumulation of *β*-catenin was remarkably reduced in compound **1** and nanoparticles NPs@CPF_2−Pt(IV) and Tf-NPs@CPF_2−Pt(IV)-treated tumor tissues in comparison with the blank and CDDP groups ($P < 0.001$).

The facts above reflected that complex **1** was potent in inhibiting the EMT progress through the Wnt/*β*-catenin pathway. In particular, nanoparticles Tf-NPs@CPF_2−Pt(IV) exerted the most satisfactory ability in reversing EMT owing to its pronouncing tumor targeting effects.

Activating Antitumor Immunity In Vivo. Immune suppressive TME is a hallmark of tumors and shows remarkable potency in accelerating the proliferation and metastasis of tumor cells.[54] Inflammation and EMT are central drivers of the immunosuppressive network. Regarding the promising performance of complex **1** and nanoparticles Tf-NPs@CPF_2−Pt(IV) in modulating the inflammatory TME and reversing EMT, their properties in activating antitumor immunity were determined by measuring the $CD3^+$ and $CD8^+$

https://doi.org/10.1021/acs.jmedchem.4c01265
J. Med. Chem. 2024, 67, 16416−16434

tumor-infiltrating lymphocytes (TILs) by the immunohistochemical staining assay, while the immunization checkpoint programmed cell death ligand 1 (PD-L1) was also tested.

The results established in Figure 12 showed that the T cell immunity was effectively provoked that the $CD3^+$- and $CD8^+$-marked T cells increased in complex **1** and nanoparticles NPs@CPF_2−Pt(IV)- and Tf-NPs@CPF_2−Pt(IV)-treated groups, which was significantly better than the blank and CDDP groups ($P < 0.001$). Meanwhile, the expression of PD-L1 was obviously suppressed in these groups ($P < 0.001$), indicating that PD-L1 inhibition was involved in the immunity activation induced by complex **1** and its nanoparticles. Notably, the tumor-targeted nanomedicine Tf-NPs@CPF_2−Pt(IV) displayed the most promising performance in activating antitumor immunity, and it improved the density of $CD3^+$ and $CD8^+$ TILs to higher levels than free complex **1** ($P < 0.001$) and NPs@CPF_2−Pt(IV) ($P < 0.001$). Therefore, the CPF platinum(IV) complex **1** and its nanoparticles, especially the tumor-targeted nanomedicine Tf-NPs@CPF_2−Pt(IV), were potent in arousing T cell antitumor immunity through inhibiting PD-L1 expression in tumors in vivo.

Pharmacokinetic Study In Vivo. To verify whether the nanotherapeutic could prolong the circulation time in vivo in comparison with the free drug, the pharmacokinetics (PK) profiles of nanoparticles NPs@CPF_2−Pt(IV) and Tf-NPs@CPF_2−Pt(IV) were evaluated to compare with free CPF_2−Pt(IV) **1** in SD rats after a single intravenous injection (i.v.) at a dose of 5 mg Pt/kg.

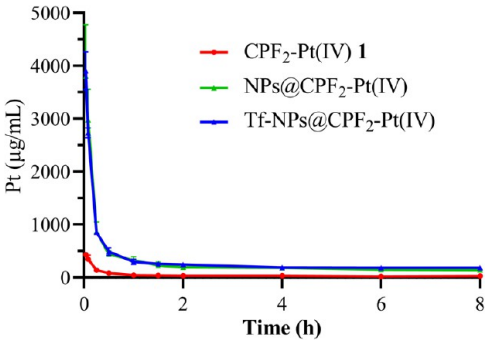

Figure 13. Pharmacokinetic curves of nanoparticles NPs@CPF_2−Pt(IV) and Tf-NPs@CPF_2−Pt(IV), as well as free complex **1** injection post a single intravenous injection at a dose of 5 mg Pt/kg to SD rats in vivo ($n = 3$).

The results in Figure 13 and Table 2 indicated that the peak plasma concentrations (C_{max}) for all three agents appeared 2 min after administration (the first time point for blood collection). The area under the plasma concentration versus time curve (AUC) for Tf-NPs@CPF_2−Pt(IV) was 9.7-fold higher than free complex **1** injection, while NPs@CPF_2−Pt(IV) also led to a 7.8 times improved AUC in blood. Then, Tf-NPs@CPF_2−Pt(IV) and NPs@CPF_2−Pt(IV) significantly prolonged the terminal elimination half-life ($T_{1/2}$) to 8.91 and 10.77 h in contrast to free complex **1** injection ($T_{1/2}$ = 4.30 h), and led to more than a 10.5-fold lower plasma clearance rate (CL) than complex **1**. Then, their volume of distribution (Vz = 1.9 and 2.7) values were lower than that of CPF_2−Pt(IV) **1** (Vz = 14.9). These results indicated that nanoparticles NPs@CPF_2−Pt(IV) and Tf-NPs@CPF_2−Pt(IV) exhibited obviously better PK profiles than the complex **1** injection, which further improved their antitumor performance in the following experiments in vivo.

Antitumor Activities In Vivo. To detect the antitumor activities of CPF platinum(IV) complexes and the nanoparticles in vivo, female BALB/c mice were employed, and tumor-bearing models were established by injection of murine 4T1 cells subcutaneously. Free complex **1** and its nanoparticles NPs@CPF_2−Pt(IV) and Tf-NPs@CPF_2−Pt(IV) were evaluated with CDDP as a positive reference drug. The drugs were administered at a dose of 2 mg Pt/kg (i.v.) three times on days 4, 7, and 10 after tumor inoculation (Figure 14a). Then, the mice were sacrificed on day 12, and the blood, tumors, and major organs, including the heart, liver, spleen, lung, and kidney, were collected.

The systemic toxicity was detected by monitoring the body weight during the experiment (Figure 14b). Free complex **1** ($P < 0.01$) and CDDP ($P < 0.001$) led to a significant loss of body weight compared with the blank group. Meanwhile, nanoparticles NPs@CPF_2−Pt(IV) and Tf-NPs@CPF_2−Pt(IV) induced rather no significant effects (P = ns). These facts highlighted that the nanoparticles based on complex **1** exhibited obviously lower toxicity than platinum(II) drug CDDP as well as free CPF platinum(IV) complex **1**, which was probably ascribed to the superior PK profiles and sustained drug release behaviors. Moreover, the low toxicity for the nanoparticles was also evidenced by the H&E staining results (Figure S10) that there were no significant histological differences observed in the liver, spleen, and kidney tissues in the nanoparticles NPs@CPF_2−Pt(IV)- and Tf-NPs@CPF_2−Pt(IV)-treated groups in comparison with the blank group.

The antitumor results depicted in Figure 14c−e manifested that free complex **1** and nanoparticles NPs@CPF_2−Pt(IV) and Tf-NPs@CPF_2−Pt(IV) exhibited effective antigrowth activities against 4T1 tumors in vivo with a tumor growth inhibition rate (TGI) of 71.3−80.4%, which were significantly more potent than CDDP (TGI = 25.7%, $P < 0.001$). Then, their remarkable antitumor potencies were also verified in the H&E staining results of tumor tissues in Figure 14f that severe cellular degeneration, necrosis, and nucleus dispersion were observed in complex **1**, NPs@CPF_2−Pt(IV)- and Tf-NPs@CPF_2−Pt(IV)-treated groups. Encouragingly, nanoparticles Tf-NPs@CPF_2−Pt(IV) with the tumor targeting motif Tf exhibited the most potent antitumor performance that it inhibited the tumor volume to 314 mm^3 at the end of the

Table 2. Pharmacokinetic Parameters C_{max}, $T_{1/2}$, AUC_{last}, CL_{obs}, and Vz_{obs} of Nanoparticles NPs@CPF_2−Pt(IV) and Tf-NPs@CPF_2−Pt(IV) and Complex 1 in SD Rats In Vivo

agents	C_{max} (μg/mL)	$T_{1/2}$ (h)	AUC_{last} (h*ng/mL)	CL_{obs} (mL/h)	Vz_{obs} (L)
CPF_2−Pt(IV) **1**	403	4.30	361	2178	14.9
NPs@CPF_2−Pt(IV)	3161	10.77	2248	145	1.9
Tf-NPs@CPF_2−Pt(IV)	3905	8.91	2433	207	2.7

https://doi.org/10.1021/acs.jmedchem.4c01265
J. Med. Chem. 2024, 67, 16416−16434

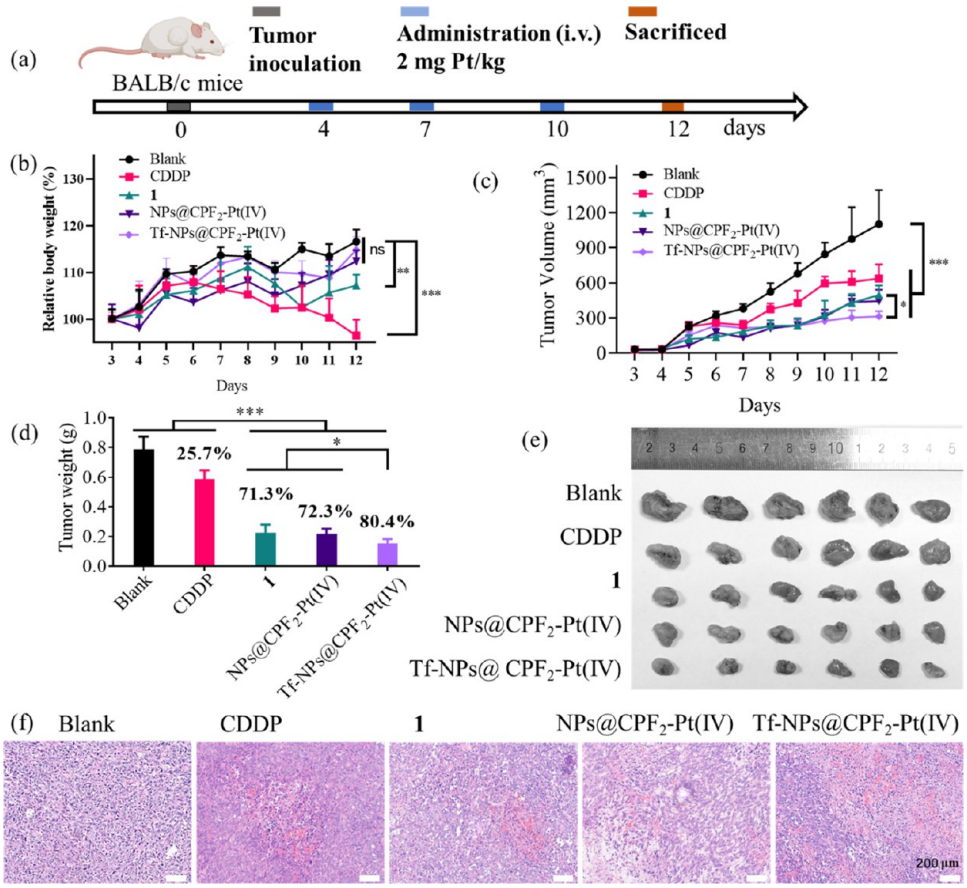

Figure 14. In vivo antitumor activities of nanomedicines NPs@CPF_2−Pt(IV), Tf-NPs@CPF_2−Pt(IV), free complex CPF_2−Pt(IV) **1**, and CDDP to 4T1 tumors in female BALB/c mice ($n = 6$). *ns*: no significant difference, $^*P < 0.05$, $^{**}P < 0.01$, and $^{***}P < 0.001$. (a) Schematic illustration of the experimental design. (b) Relative body weight of the mice during the treatment. (c) Tumor growth as a function of time. (d) Tumor weight of each group at the end of the experiment. The TGI of the tested drugs in comparison with the blank group was depicted above the column [TGI = (1 − tumor weight of the drug-treated group/tumor weight of blank group) × 100%]. (e) Image of tumors after the mice were sacrificed. (f) H&E staining of tumor tissues.

experiment and led to a higher TGI = 80.4% than free complex **1** (496 mm^3, TGI = 71.3%, $P < 0.05$) and NPs@CPF_2−Pt(IV) (444 mm^3, TGI = 72.3%, $P < 0.05$), which was mainly ascribed to the more promising tumor targeting capacity in vivo (see the Tumor Targeting Properties In Vivo).

Summarily, complex **1** exhibited effective antitumor activities in vivo, which was more promising than CDDP. Then, the preparation of nanoparticles with biocompatible $DSPE\text{-}PEG_{2000}$ provided a promising way to further elevate the antitumor efficacy and decrease the toxicity of CPF platinum-(IV) conjugates. Especially, the Tf-modified nanomedicine Tf-NPs@CPF_2−Pt(IV) displayed the most promising antitumor potency in vivo, which was more significant and less toxic than CDDP and free complex **1** as well as nanoparticles NPs@CPF_2−Pt(IV).

Tumor Targeting Properties In Vivo. The tumor targeting properties of antitumor agents were an important factor in influencing the antitumor potency, especially toward malignant metastatic tumors. Herein, the tumor targeting properties of nanoparticles Tf-NPs@CPF_2−Pt(IV) and NPs@CPF_2−Pt(IV) were tested on female BALB/c mice bearing 4T1 tumors with DiD as a fluoresce probe, which was often loaded in nanoparticles as a tracer for detecting the biodistribution and metabolism of drugs after systemic administration in mice. The DiD-labeled nanoparticles DiD-NPs@CPF_2−Pt(IV) and DiD-Tf-NPs@CPF_2−Pt(IV) were intravenously injected into mice (2 mg of Pt/kg), using the injection of the mixture of free complex **1** with DiD (DiD-**1**) as a control. The fluorescence intensity was monitored using an IVIS optical imaging system.

As shown in Figure 15a, the accumulation of DiD-NPs@CPF_2−Pt(IV) and DiD-Tf-NPs@CPF_2−Pt(IV) in tumors increased gradually in 24 h after drug administration and was obviously higher than that of free DiD-**1**, which was probably attributed to the EPR effect.[55] Notably, the fluorescence in the DiD-Tf-NPs@CPF_2−Pt(IV) group reached a higher level than DiD-NPs@CPF_2−Pt(IV) after 1 h injection, and this trend was mainly ascribed to the quick combination of Tf with the overexpressed Tf receptor on the membrane of tumor cells. Then, the mice were sacrificed at 24 h, and tumors were collected for ex vivo imaging. The fluorescence intensity of tumors shown in Figure 15b,d further demonstrated the higher accumulation level for DiD-Tf-NPs@CPF_2−Pt(IV) in tumors and that its fluorescence intensity was remarkably higher than DiD-**1** ($P < 0.001$) and DiD-NPs@CPF_2−Pt(IV) ($P < 0.05$). Then, the distribution analysis of drugs in tumors and organs (heart, liver, spleen, lung, and kidney; Figure 15c,e) manifested that DiD-Tf-NPs@CPF_2−Pt(IV) accumulated in tumors at a dramatically higher portion (30.2%) than NPs@CPF_2−Pt(IV) (16.9%) and DiD-**1** (0.3%). These trends indicated that the

https://doi.org/10.1021/acs.jmedchem.4c01265
J. Med. Chem. 2024, 67, 16416−16434

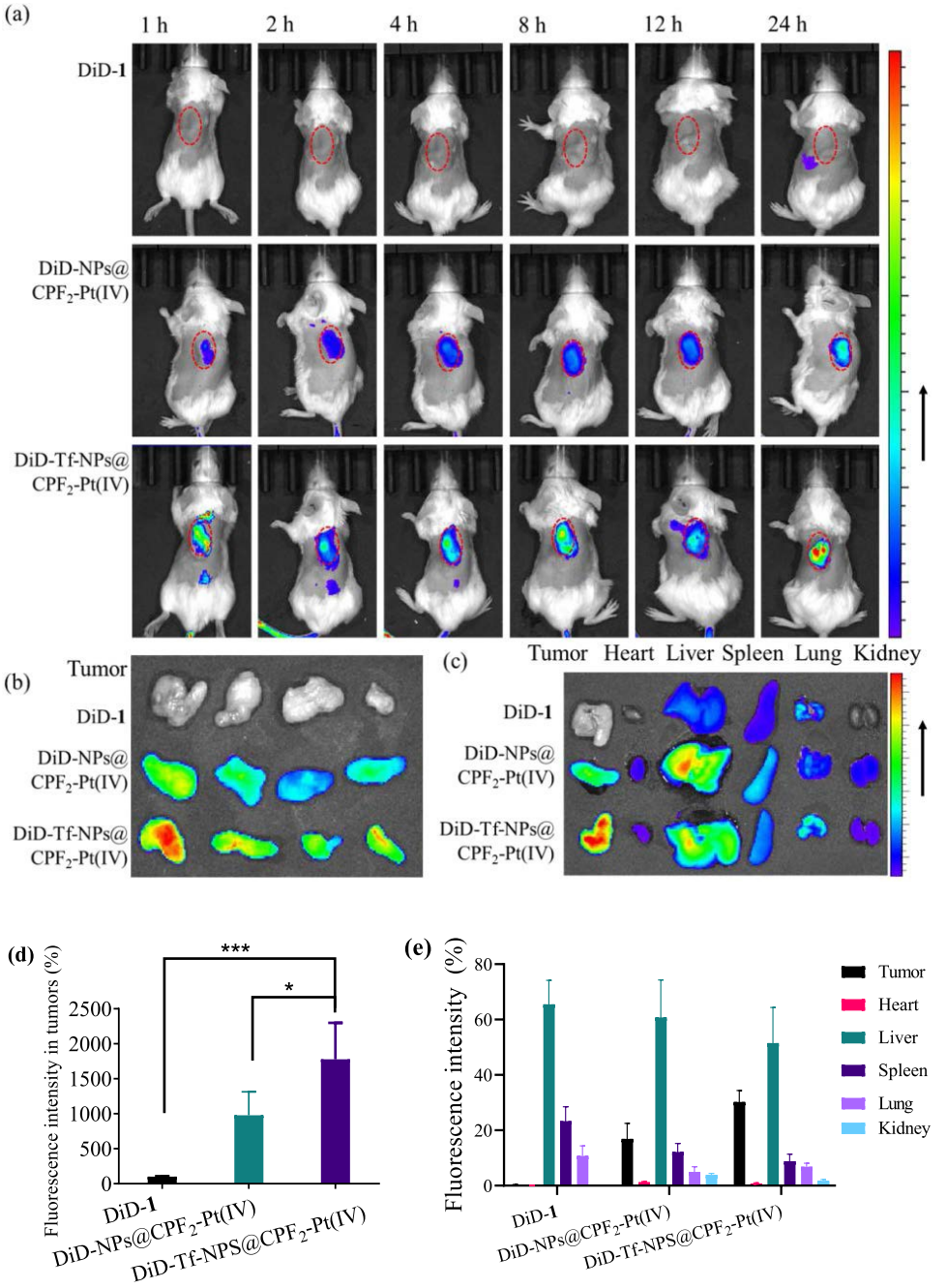

Figure 15. Biodistribution and targeting study of DiD-labeled nanoparticles DiD-NPs@CPF_2−Pt(IV) and DiD-Tf-NPs@CPF_2−Pt(IV) and the mixture of DiD with free complex **1** (DiD-**1**) in vivo (n = 4). (a) Mice bearing 4T1 tumor grafts were injected (i.v.) with the DiD-labeled agents followed by dynamic scanning using an IVIS optical imaging system at 1, 2, 4, 8, 12, and 24 h postinjection. (b) Ex vivo images of the tumor tissues and (d) the relative fluorescence intensity in tumors at the end of the experiment. (c) Ex vivo images of the tissues including the tumor, heart, liver, spleen, lung, and kidney and (e) the distribution of drugs in these tissues (relative fluorescence intensity = (fluorescence intensity in specified tissues/fluorescence intensity in all tissues including the tumor, heart, liver, spleen, lung, and kidney) × 100%). *P < 0.05 and ***P < 0.001.

introduction of Tf into the nanoparticles of CPF_2−Pt(IV) **1** to form Tf-NPs@CPF_2−Pt(IV) was a promising strategy to improve tumor targeting effects.

The evaluation of drug accumulation was another direct method to determine the tumor targeting properties of antitumor agents in vivo. Subsequently, the drug accumulation of Tf-NPs@CPF_2−Pt(IV) in tumors was measured using the AAS assay (tissues were obtained from the antitumor activities in vivo). The results in Figure S11 confirmed that nanoparticles Tf-NPs@CPF_2−Pt(IV) accumulated in tumor tissues at a higher level than NPs@CPF_2−Pt(IV) (P < 0.05) and free complex **1** (P < 0.001) as well as CDDP (P < 0.001), which was mainly in accordance with the IVIS optical imaging results.

Overall, the results of IVIS optical imaging and AAS assays disclosed that the tumor-targeted nanoparticles Tf-NPs@CPF_2−Pt(IV) designed in this work possessed prominent properties in targeting tumor tissues through the Tf motif and EPR effect, which further affected the antitumor activities, especially toward metastatic tumors.

https://doi.org/10.1021/acs.jmedchem.4c01265
J. Med. Chem. 2024, 67, 16416−16434

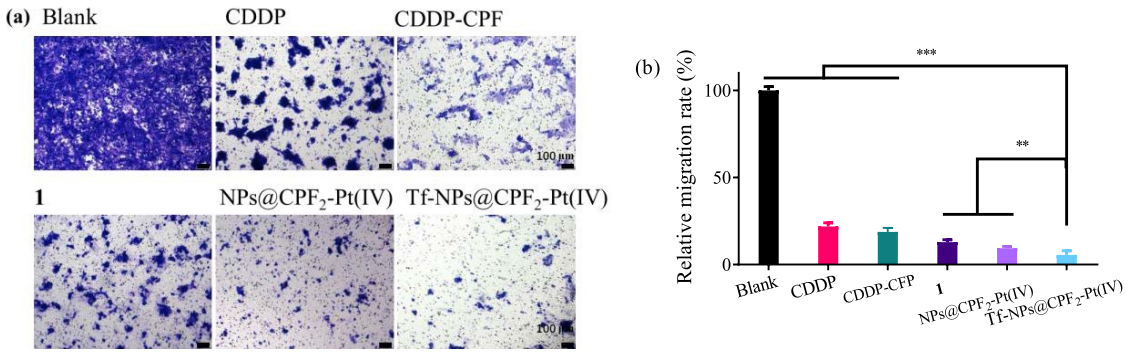

Figure 16. Evaluation of the migration inhibition properties of CDDP (5 μM), CDDP−CPF (5 μM/10 μM), complex **1** (5 μM), NPs@CPF_2−Pt(IV) (5 μM), and Tf-NPs@CPF_2−Pt(IV) (5 μM) to 4T1 cells using the transwell assay in vitro. Tumor cells were treated with platinum drugs for 24 h, and the untreated cells were set as blank. (a) Representative images. (b) Analysis of the relative migration rate. $^{**}P < 0.01$ and $^{***}P < 0.001$.

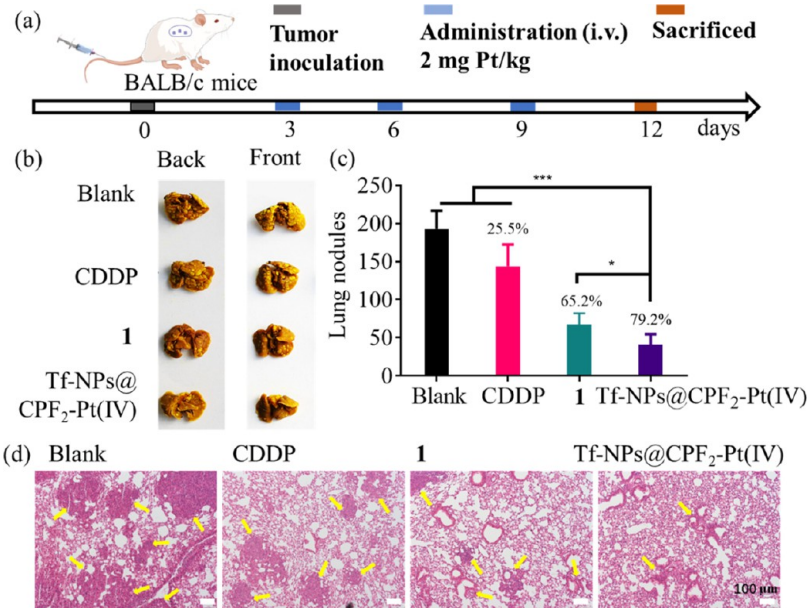

Figure 17. Pulmonary metastasis inhibition properties of nanoparticles Tf-NPs@CPF_2−Pt(IV), complex **1**, and CDDP against 4T1 tumors in vivo ($n = 5$). $^{*}P < 0.05$ and $^{***}P < 0.001$. (a) Schematic illustration of the experimental design. (b) Representative photographs of the front and back sides of lungs from each group at the end of the experiment. (c) Lung nodules in each group. The inhibition rate in comparison with the blank group was depicted above the column. (d) H&E staining of lung metastasis nodules. Nodules were indicated by arrows.

Antimetastatic Activities In Vitro and In Vivo. Encouraged by the prominent antitumor activities, the antimetastatic potency of nanomedicine Tf-NPs@CPF_2−Pt(IV) was evaluated by the transwell and wound healing assays in vitro and the pulmonary metastasis models in vivo.

The transwell results in Figure 16 indicated that Tf-NPs@CPF_2−Pt(IV) was effective in suppressing the migration of tumor cells, which was superior to NPs@CPF_2−Pt(IV) ($P < 0.01$), free complex **1** ($P < 0.01$), and CDDP ($P < 0.001$), as well as the mixture CDDP−CPF ($P < 0.001$). Then, the wound healing assay (Figure S12) further evidenced the potent antimetastatic effects of Tf-NPs@CPF_2−Pt(IV), indicating that it caused a rather lower wound healing rate than NPs@CPF_2−Pt(IV) ($P < 0.001$), CPF_2−Pt(IV) ($P < 0.001$), CDDP ($P < 0.001$), and the mixture CDDP−CPF ($P < 0.001$). Obviously, Tf-NPs@CPF_2−Pt(IV) was potent in suppressing the metastasis of tumor cells in vitro.

Pulmonary metastasis is one of the most common forms of tumor metastasis, and pulmonary metastasis models were usually employed to determine the antimetastatic ability of drugs in vivo. Herein, the pulmonary metastasis models were established by injecting 4T1 cells via the tail vein of female BALB/c mice. The drugs including Tf-NPs@CPF_2−Pt(IV) and free complex **1** were administrated (i.v.) on days 3, 6, and 9 at a dosage of 2 mg Pt/kg (Figure 17a). Then, the mice were sacrificed on day 12. The lung tissues were collected, and the nodules on the surface of the lung tissues were counted to determine the antimetastasis potency of the drugs. Results in Figure 17b,c reflected that Tf-NPs@CPF_2−Pt(IV) was potent in inhibiting the metastasis of the tumor cells in vivo, which were significantly more effective than CDDP ($P < 0.001$). Encouragingly, nanoparticles Tf-NPs@CPF_2−Pt(IV) possessed an even higher inhibition rate of 79.2% than free CPF_2−Pt(IV) **1** (65.2%, $P < 0.05$). Then, the H&E staining images of lung tissues in Figure 17d depicted that fewer and smaller lung metastatic nodules were observed in the Tf-NPs@CPF_2−Pt(IV)-treated group than in the blank, CDDP, and free conjugate **1**-treated groups, which further verified the

https://doi.org/10.1021/acs.jmedchem.4c01265
J. Med. Chem. 2024, 67, 16416−16434

promising antimetastatic properties of nanoparticles Tf-NPs@CPF_2−Pt(IV) in vivo. Totally, the antimetastatic results in vitro and in vivo demonstrated that Tf-NPs@CPF_2−Pt(IV) was of great potential to be developed as novel antimetastatic drugs.

CONCLUSIONS

The metastasis of tumor cells is still the leading cause of death in cancer patients. The inflammatory TME is a central driver of tumor metastasis and is tightly associated with the promotion of EMT and immune suppression in tumor tissues. Moreover, poor tumor targeting is a key constraint to the efficacy of platinum drugs in the clinic. In this work, tumor targeting nanoparticles based on CPF platinum(IV) complexes were developed as antiproliferative and antimetastatic drugs. Platinum(IV) complex CPF_2−Pt(IV) **1** with dual CPF ligands exerted superior antitumor activities to the corresponding mono ligand conjugate CPF−Pt(IV) **2** and showed great potential in overcoming the drug resistance of CDDP and decreasing toxicity. Then, nanoparticles NPs@CPF_2−Pt(IV) and Tf-NPs@CPF_2−Pt(IV) based on complex **1** were developed. Both nanoparticles released the active ingredient CPF_2−Pt(IV) **1** in a sustained manner; meanwhile, they also exerted remarkably better PK properties than free CPF_2−Pt(IV) **1** in vivo with improved AUC and terminal elimination half-life, which prolonged the exposure of tumors to chemotherapeutics. Notably, Tf-NPs@CPF_2−Pt(IV) modified by the Tf motif displayed satisfactory tumor targeting effects over free complex **1** ($P < 0.001$) and NPs@CPF_2−Pt(IV) ($P < 0.05$) in vivo. Subsequently, it exhibited promising antitumor competency in vivo and led to a higher TGI of 80.4% against 4T1 tumors than CDDP (TGI = 25.7%, $P < 0.001$), free complex **1** (TGI = 71.3%, $P < 0.05$), and nanoparticles NPs@CPF_2−Pt(IV) (TGI = 72.3%, $P < 0.05$). More encouragingly, Tf-NPs@CPF_2−Pt(IV) also possessed pronounced antimetastatic effects in vivo, indicating that it significantly suppressed the nodules in the pulmonary metastasis models with a high inhibition rate of 79.2% relative to the blank group ($P < 0.001$), which was more potent than CDDP (25.5%, $P < 0.001$) and free complex **1** (65.2%, $P < 0.05$). The mechanism detection disclosed that Tf-NPs@CPF_2−Pt(IV) could release active ingredient **1** gradually, causing serious DNA damage after reduction to platinum(II) form in reducing TME with the upregulation of γ-H2AX and P53. Then, obvious mitochondria-mediated apoptosis was initiated through the Bcl-2/Bax/caspase3 pathway accompanied by the induction of $\Delta\Psi_m$ collapse and ROS production. Moreover, the chronic inflammation in tumors was alleviated by Tf-NPs@CPF_2−Pt(IV) by downregulating the expression of COX-2 and MMP9 and subsequently inhibiting the secretion of inflammatory cytokines TNF-α and IL-6. Following that, the EMT progress in tumors was remarkably suppressed through the Wnt/β-catenin/EMT axis, which was demonstrated by the upregulation of *E*-cadherin and downregulation of *N*-cadherin, vimentin, Snail1, β-catenin, cyclin D1, and *c*-Myc. The satisfactory antitumor performance of Tf-NPs@CPF_2−Pt(IV) was also associated with the immunity activation by blocking the immune checkpoint PD-L1 in tumors ($P < 0.001$), and the density of $CD3^+$ and $CD8^+$ TILs increased remarkably in the Tf-NPs@CPF_2−Pt(IV) group in comparison with the blank, CDDP, free complex **1**, and nanoparticles NPs@CPF_2−Pt(IV)-treated groups ($P < 0.001$).

Overall, a potent nanodrug (Tf-NPs@CPF_2−Pt(IV)) based on the CPF platinum(IV) hybrid with promising antiproliferative and antimetastatic properties was developed in this work, and the advantages of this nanoagent were summarized as follows: (a) Tf-NPs@CPF_2−Pt(IV) exhibited superior release behaviors and pharmacokinetic profiles over free platinum(IV) conjugate CPF_2−Pt(IV) **1**, which was mainly ascribed to the NDDS, and further possessed mitigated side effects both in vitro and in vivo. (b) Tf, utilized as a tumor targeting motif, effectively transported the cytotoxic platinum(IV) conjugate to tumor tissues, especially to the metastatic sites, thereby improving the antitumor potency. (c) Hybrid CPF_2−Pt(IV) **1**, as the active ingredient of Tf-NPs@CPF_2−Pt(IV), imbued the nanoparticles with a multispecific antitumor mechanism of inhibiting inflammation, reversing EMT, and stimulating antitumor immunity, in addition to causing DNA damage. These comprehensive advantages contributed synergistically to the effective antiproliferative and antimetastatic activities of nanoparticles Tf-NPs@CPF_2−Pt(IV) and reduced toxicities. The findings of this study provided a practical strategy for improving tumor targeting properties, enhancing antitumor activities, and minimizing toxicities of the platinum complexes. These results hold significant implications for future efforts in developing new antitumor drugs based on NSAID platinum-(IV) conjugates, particularly for the treatment of metastatic cancers.

EXPERIMENTAL SECTION

General. Materials CDDP and OXP were purchased from Boyuan Pharmaceutical Co., Ltd. (Jinan, China). Other chemicals were purchased from Sigma, J&K, Aladdin, Macklin, and Innochem and were used without further purification unless specifically mentioned. The reactions were performed under an atmosphere of nitrogen in flame-dried glassware with magnetic stirring unless specifically noted. The NMR spectra were recorded on a Bruker spectrometer operating at 500 MHz for ^{1}H NMR and 126 MHz for ^{13}C NMR. The mass spectra (MS) were carried out on a Shimadzu LC-MS/MS 8040 mass spectrometer with ESI ionization. The high-resolution mass spectra (HRMS) were recorded on a Waters G2-XS QTof mass spectrometer. Atomic absorption spectroscopy (AAS) was tested on a Shimadzu AA-6880. Flow cytometric measurements were carried out with a Millipore Guava easyCyte 8HT flow cytometer. The HPLC analysis was performed on a Thermo Ultimate 3000 RS or Shimadzu LC-20A spectrometer. All compounds were >95% pure as determined by HPLC analysis.

Synthetic Procedure. *Preparation of Oxoplatin.* A suspension of CDDP (1.0 g, 3.3 mmol) in 30 mL of distilled water was stirred at room temperature. Then, 50 mL of H_2O_2 (30%) was added dropwise, and the suspension was stirred at 60 °C for 4 h. The resultant mixture was recrystallized at 4 °C overnight. The crude product was obtained as a yellow solid after filtration. The further recrystallization in water afforded pure oxoplatin as yellow crystals (0.75 g, 68%).

Preparation of Compound CPF_2−Pt(IV) (1). CPF (274 mg, 0.90 mmol) and TBTU (289 mg, 0.90 mmol) were dissolved in 5 mL of dry *N*,*N*-dimethylformamide (DMF) and stirred at room temperature for 15 min. Then, TEA (125 μL, 0.90 mmol) was added, and the mixture was stirred for another 15 min. After that, oxoplatin (100 mg, 0.30 mmol) was added. The mixture was stirred at 50 °C for 48 h in the dark under a nitrogen atmosphere. After the reaction was completed, the solvent was removed under vacuum, and the crude product was purified by silica gel column chromatography to afford compound **1** as a yellow solid (78.0 mg, 30%). Its purity was 98.8%, as determined by HPLC (MeOH/H_2O = 85/15). Melting point: 173.5−174.5 °C. ^{1}H NMR (500 MHz, DMSO-d_6) δ 11.29 (s, 2H), 8.16 (d, J = 2.2 Hz, 2H), 8.03 (d, J = 8.2 Hz, 2H), 7.53−7.42 (m, 4H), 7.38−7.30 (m, 2H), 7.17 (d, J = 8.2 Hz, 2H), 6.54 (br, 6H), 3.87 (d, J = 7.1 Hz, 2H), 1.45−1.39 (m, 6H). ^{13}C NMR (126 MHz,

https://doi.org/10.1021/acs.jmedchem.4c01265
J. Med. Chem. 2024, 67, 16416−16434

DMSO-d_6) δ: 182.6, 141.3, 140.9, 138.8, 125.3, 124.2, 123.2, 120.6, 120.6, 120.0, 119.7, 112.7, 110.5, 47.5, 20.8. MS-ESI: calcd for $[M + H]^+$: 844 (M = $C_{30}H_{28}Cl_4N_4O_4Pt$), found: 844. HRMS: calcd for $[M + Na]^+$: 866.0410 (M = $C_{30}H_{28}Cl_4N_4O_4Pt$), found: 866.0419.

*Preparation of Compound CPF−Pt(IV) (**2**).* CPF (82 mg, 0.3 mmol) and TBTU (96 mg, 0.3 mmol) were dissolved in 5 mL of dry DMF and stirred at room temperature for 15 min. Then, TEA (42 μL, 0.3 mmol) was added, and the mixture was stirred for another 15 min. After that, oxoplatin (100 mg, 0.3 mmol) was added. The mixture was stirred at 50 °C for 48 h in the dark under a nitrogen atmosphere. After the reaction was completed, the solvent was removed under vacuum, and the crude product was purified by silica gel column chromatography to afford compound **2** as a yellow solid (43.0 mg, 24%). Its purity was 99.2% as determined by HPLC (MeOH/H_2O = 85/15). Melting point: 159.8−160.8 °C. ^{1}H NMR (500 MHz, DMSO-d_6) δ 11.34 (s, 1H), 8.17 (d, J = 2.1 Hz, 1H), 8.04 (d, J = 8.2 Hz, 1H), 7.49−7.43 (m, 2H), 7.38−7.32 (m, 1H), 7.19−7.13 (m, 1H), 6.47 (br, 6H), 3.95 (d, J = 7.2 Hz, 1H), 1.43 (d, J = 7.1 Hz, 3H). ^{13}C NMR (126 MHz, DMSO-d_6) δ: 181.7, 141.0, 140.9, 138.8, 125.4, 124.1, 123.2, 120.7, 120.6, 120.0, 119.7, 112.8, 110.6, 46.6, 21.0. MS-ESI: calcd for $[M + Na]^+$: 590 (M = $C_{15}H_{18}Cl_3N_3O_3Pt$), found: 590. HRMS: calcd for $[M + Na]^+$: 610.9959 (M = $C_{15}H_{18}Cl_3N_3O_3Pt$), found: 610.9954.

Preparation of Nanoparticles NPs@CPF$_2$−Pt(IV). Generally, complex CPF$_2$−Pt(IV) **1** was codissolved with DSPE-PEG$_{2000}$ (**1**:DSPE-PEG$_{2000}$ = 1:1, mol/mol) in 0.5 mL of DMF. Then, the mixture was dropwise added to PBS (20 mL) under vigorous stirring. The resulting mixture was further stirred for 15 min. After that, the obtained nanoparticles were homogenized by a D-3L homogenizer (PhD) at optimal homogenization conditions of 100 MPa for 60 min to reduce the size. The solution was dialyzed (MWCO 8−14 kDa) twice against deionized water to remove the organic solvent. Nanoparticles NPs@CPF$_2$−Pt(IV) were obtained. The nanoparticles at other CPF$_2$−Pt(IV) **1**/DSPE-PEG$_{2000}$ ratios of 7:1, 5:1, 3:1, and 1:3 were prepared in the same way. Their particle size distributions were determined using DLS. The encapsulation efficiency of complex **1** in the nanoparticles was determined by AAS. The TEM images of the nanoparticles were taken after freeze-drying.

Preparation of Nanoparticles Tf-NPs@CPF$_2$−Pt(IV). Tf-modified DSPE-PEG$_{2000}$ (DSPE-PEG$_{2000}$-Tf) was added to the solution of nanoparticles NPs@CPF$_2$−Pt(IV) at a ratio of 3:4 (mol/mol). The mixture was incubated at 30 °C for 1 h. Nanoparticles Tf-NPs@CPF$_2$−Pt(IV) were obtained, and the particle size distribution was determined using DLS. The TEM images of the nanoparticles were taken after freeze-drying. Subsequently, the binding ratio of Tf to NPs@CPF$_2$−Pt(IV) was detected using a BCA kit (Beyotime Biotechnology, China).

Releasing Behavior of NPs@CPF$_2$−Pt(IV) and Tf-NPs@CPF$_2$−Pt(IV). The release behavior of nanoparticles NPs@CPF$_2$−Pt(IV) and Tf-NPs@CPF$_2$−Pt(IV) was performed in PBS. A solution of complex **1** in media of PBS containing 5% DMF was prepared as an injection to compare with the nanoparticles. Briefly, 5 mL of nanoparticles or injection containing the same concentration of complex **1** (0.5 mM) was transferred into dialysis bags (MWCO 8−14 kDa), immersed into 100 mL of PBS media containing 0.5% w/v sodium dodecyl sulfate (SDS), and stirred at 100 rpm at 37 °C. At a set point of time, the release solution (3 mL) was withdrawn, followed by being substituted with the same volume of fresh media. The experiments were performed for 72 h. The concentration of complex **1** in the collected solution was determined using the AAS assay by measuring the Pt contents. The releasing behavior was determined based on three parallel experiments.

Preparation of DiD-Labeled Nanoparticles DiD-NPs@CPF$_2$−Pt(IV) and DiD-Tf-NPs@CPF$_2$−Pt(IV). The DiD was encapsulated in the nanoparticles accompanied by complex **1**. Complex **1**, DSPE-PEG$_{2000}$ (**1**:DSPE-PEG$_{2000}$ = 1:1, mol/mol), and DiD (1% of DSPE-PEG$_{2000}$, w/w) were dissolved in DMF (0.5 mL). Then, the mixture was added dropwise into 20 mL of PBS under vigorous stirring. The resultant mixture was further stirred for 15 min. After that, the obtained nanoparticles were homogenized by a D-3L homogenizer (PhD) at 100 MPa for 60 min to reduce the particle size. DiD-encapsulated nanoparticles DiD-NPs@CPF$_2$−Pt(IV) were obtained. Then, DSPE-PEG$_{2000}$-Tf was added to the solution of nanoparticles DiD-NPs@CPF$_2$−Pt(IV) at a ratio of 3:4 (mol/mol), and the mixture was incubated at 30 °C for 1 h. Nanoparticles DiD-Tf-NPs@CPF$_2$−Pt(IV) were obtained.

Stability of Nanoparticles NPs@CPF$_2$−Pt(IV) and Tf-NPs@CPF$_2$−Pt(IV). Nanoparticles NPs@CPF$_2$−Pt(IV) and Tf-NPs@CPF$_2$−Pt(IV) were stored at 4 °C for 21 days to evaluate their storage stability via detecting the particle size by DLS at 0, 1, 3, 5, 7, 14, and 21 days. The experiments were conducted in triplicates.

Cell Culture. Cell strains of human lung cancer (A549), CDDP-resistant human lung cancer (A549R), murine breast cancer (4T1), human liver cancer (HepG2), and human normal liver cell line (LO2) were stored in the laboratory and originated from American Type Culture Collection (ATCC) and Pricella Biotechnology Co., Ltd. (Wuhan, China). The cells were cultured either in DMEM (for HepG2) or in RPMI1640 (for A549, A549R, LO2, and 4T1 cells) media containing 10% fetal bovine serum (FBS) and 1% penicillin/streptomycin in a humidified atmosphere containing 5% CO_2 at 37 °C. All cell culture reagents were purchased from Solarbio (Beijing, China).

Animals. The experiments in vivo were evaluated on immune component female BALB/c mice (18−20 g) regarding the immune promoting properties of the CPF platinum(IV) agents, which were purchased from Pengyue Experimental Animal Company (Jinan, China). Female SD rats (200−220 g) were used in pharmacokinetic studies, which were purchased from Henan Skobes Biotechnology Co., LTD (Henan, China). All animals were kept under standard conditions (12/12 h day/night cycle, 23 ± 2 °C) and given free access to diet and water. The experiments were carried out in strict accordance with the NIH guidelines for the care and use of laboratory animals (NIH Publication No. 8023, revised 1978) and were approved by the Institute Animal Ethics Committee of Liaocheng University.

Antiproliferative Activity Assays In Vitro. An MTT assay was applied to detect the antiproliferative activities of conjugates **1** and **2** and nanoparticles NPs@CPF$_2$−Pt(IV) and Tf-NPs@CPF$_2$−Pt(IV), with platinum(II) drugs CDDP and OXP, and platinum(IV) drug STP as references. The CPF ligand and the mixture of CDDP and CPF (CDDP−CPF) with a molar ratio of 1:2 were also evaluated. Four tumor cell lines, including human lung cancer (A549), CDDP-resistant human lung cancer (A549R), murine breast cancer (4T1), and human liver cancer (HepG2), and one human normal liver cell line (LO2) were evaluated. Briefly, tumor cells suspended in 100 μL of the medium were seeded in 96-well microtiter plates (5×10^3/well) and preincubated overnight. Then, drugs with stepwise diluted concentrations in 100 μL of the medium were added. The tumor cells were treated with drugs for 48 h. After that, 20 μL of a freshly prepared MTT solution in PBS (5 mg/mL) was added, and the mixture was incubated for another 4 h. Subsequently, the culture was removed, and dimethyl sulfoxide (DMSO, 150 μL) was added. The optical density of each well was measured by a microplate spectrophotometer (λ = 490 nm). The antiproliferative data were given as IC_{50} values based on three parallel experiments.

Uptake Analysis Assay. The accumulation of drugs in vitro and in vivo was detected by measuring the Pt contents using the AAS assay. To determine the uptake in whole cells, 4T1 cells (6×10^6) were seeded in a 10 cm Petri dish and preincubated for 4 h. Then, CDDP, complexes **1** and **2**, and nanoparticles NPs@CPF$_2$−Pt(IV) and Tf-NPs@CPF$_2$−Pt(IV) were added, and the cells were further incubated for 24 h. Subsequently, the cells were collected and washed with PBS three times. The uptake levels were measured by AAS after digestion with 70% HNO_3. To evaluate the subdistribution of drugs in tumor cells, 4T1 cells were treated in the same way as mentioned above, and the DNA, membrane, and cytoplasm were isolated with an extraction kit purchased from Beyotime Biotechnology (China). The Pt concentration in each counterpart was measured by AAS after digestion with 70% HNO_3 to calculate the distribution of drugs in 4T1 cells. To measure the drug accumulation in tumor tissues, 0.1 g

https://doi.org/10.1021/acs.jmedchem.4c01265
J. Med. Chem. 2024, 67, 16416−16434

of tissues of the blank, free complex **1**, CDDP, and nanoparticles NPs@CPF_2−Pt(IV) and Tf-NPs@CPF_2−Pt(IV) groups from the antitumor experiments in vivo were digested with 70% HNO_3 and measured by AAS. The results were given based on three parallel experiments.

Mitochondrial Membrane Potential Experiment—JC-1 Assay. In brief, 4T1 cells (4×10^5) were seeded in six-well plates and preincubated overnight. Then, CDDP (5 μM), CDDP−CPF (5 μM/10 μM), complex **1** (5 μM), NPs@CPF_2−Pt(IV) (5 μM), and Tf-NPs@CPF_2−Pt(IV) (5 μM) were added, and the cells were further incubated for 24 h. The untreated cells were set as the blank group. Subsequently, the cells were collected and stained with JC-1 according to the instructions provided in the kit (Solarbio, China). After that, the cells were collected and analyzed by a flow cytometric assay.

Purity, Stability, Reduction Potential, and DNA Binding Properties—HPLC Assay. The purity, stability, reduction potential, and DNA binding properties of CPF platinum(IV) complexes were tested by the HPLC method using an Agilent C18 column (250 mm × 4.6 mm, 5 μm) on a Thermo Ultimate 3000 RS.

The purity, stability, and reduction potential were evaluated at a fixed eluant composition (85% methanol/15% water), a flow rate of 1.0 mL/min, and a λ of 300 nm. The injection volume was 10 μL. For purity detection, solutions of complexes **1** and **2** (0.5 mM) were prepared and tested. For stability detection in biological media, a solution of complex **1** (0.5 mM) in RPMI1640 was prepared and incubated at 37 °C, and the spectra were recorded for 48 h. For reduction potential detection, a solution of complex **1** (0.5 mM) in RPMI1640 in the presence of AsA (1 mM, similar to that in the TME) was prepared and incubated at 37 °C, and the spectra were recorded for 48 h.

The DNA binding properties of CPF platinum(IV) complex **1** were determined by preparing a solution of complex **1** (0.5 mM) in RPMI1640 in the presence of AsA (1 mM) and 5′-GMP (3 mM, a model of the DNA base). The chromatogram was as follows (λ = 300 nm): Phase A was water and phase B was methanol; 10% phase B (stationary from 0 to 5 min); 10 to 60% phase B (a linear increase from 5 to 25 min); 60 to 90% phase B (a linear increase from 25 to 26 min); and 90% phase B (stationary from 26 to 34 min). The flow rate was 1.0 mL/min. The HPLC spectra were recorded at 2 and 48 h. The new platinate GMP peak in the HPLC spectra demonstrated DNA binding properties.

Detection of TNF-α and IL-6 in Tumor Tissues—ELISA Assay. The levels of inflammatory cytokines TNF-α and IL-6 in tumor tissues in vivo were detected using ELISA assay kits according to the protocols suggested by the manufacturer (Meimian Biotechnology, Jiangsu, China). The tumor tissues of the blank, free complex **1**, CDDP, and nanoparticles NPs@CPF_2−Pt(IV) and Tf-NPs@CPF_2−Pt(IV) groups were obtained from the antitumor experiments in vivo. The results were calculated based on three parallel experiments.

Transwell Assay. The transwell assay was carried out using a 24-well chamber (Costar 3422) containing inserts (8 μm pores). The serum-deprived 4T1 cells (48 h) suspended in RPMI1640 medium (5×10^4 cells in 0.2 mL) were seeded in the upper compartment of the chamber, and the culture media containing 10% FBS (0.6 mL) with or without CDDP (5 μM), CDDP−CPF (5 μM/10 μM), complex **1** (5 μM), NPs@CPF_2−Pt(IV) (5 μM), and Tf-NPs@CPF_2−Pt(IV) (5 μM) were added in the lower compartment. The cells were incubated for 24 h, fixed with 4% paraformaldehyde for 20 min, and stained with 0.1% crystal violet for 20 min. After that, the nonmigrating cells in the upper chamber were scraped away gently, and the migrated cells in the lower surface were imaged with an inverted microscope (Olympus). The migration inhibition properties were evaluated based on five random visual fields.

Wound Healing Assay. The serum-deprived 4T1 cells (48 h) were suspended in the RPMI1640 medium with 1% FBS and seeded in six-well culture plates (4×10^5 cells/well). Then, a wound was generated after the cells grew to 90% confluency. Then, CDDP (5 μM), CDDP−CPF (5 μM/10 μM), complex **1** (5 μM), NPs@CPF_2−Pt(IV) (5 μM), and Tf-NPs@CPF_2−Pt(IV) (5 μM) in the RPMI1640 medium with 1% FBS were added. The untreated cells were set as a blank group. The cells were further incubated for 24 h, and the scratch of cells was photographed with an inverted microscope (Olympus) at 0, 12, and 24 h. The wound healing rate was analyzed by ImageJ based on five random visual fields.

Apoptosis Experiment—Annexin V-FITC/PI Assay. The apoptosis-inducing properties were evaluated by an Annexin V-FITC/PI double staining assay. Briefly, 4T1 cells were seeded in 6-well culture plates (4×10^5 cells/well) and preincubated overnight. Then, drugs CDDP (5 μM), CDDP−CPF (5 μM/10 μM), complex **1** (5 μM), NPs@CPF_2−Pt(IV) (5 μM), and Tf-NPs@CPF_2−Pt(IV) (5 μM) were added, and the cells were further incubated for 24 h. The untreated cells were set as a blank group. After that, the cells were trypsinized, collected, and stained with Annexin V-FITC and PI according to the operation manual of the detection kit (Beyotime Biotechnology, China). Subsequently, the cells were analyzed by flow cytometry.

ROS Experiment—DCFH-DA Assay. The ROS-inducing properties were evaluated by the DCFH-DA staining assay. In brief, 4T1 cells were seeded in 6-well culture plates (4×10^5 cells/well) and preincubated overnight. Then, drugs CDDP (5 μM), CDDP−CPF (5 μM/10 μM), complex **1** (5 μM), NPs@CPF_2−Pt(IV) (5 μM), and Tf-NPs@CPF_2−Pt(IV) (5 μM) were added, and the cells were further incubated for 24 h. The untreated cells were set as a blank group. After that, the cells were trypsinized, collected, and stained with DCFH-DA according to the operation manual of the detection kit (Beyotime Biotechnology, China). Subsequently, the cells were analyzed by flow cytometry and photographed with an inverted microscope.

Western Blot Assay. The expression of proteins was detected by a western blot assay. Briefly, 4T1 cells were treated by drugs CDDP (5 μM), CDDP−CPF (5 μM/10 μM), complex **1** (5 μM), and Tf-NPs@CPF_2−Pt(IV) (5 μM) for 24 h, and the untreated cells were set as a blank group. Then, the cells were harvested and lysed with Cell Lysis Solution (Sangon Biotec, China). The total protein was collected and determined with a BCA protein assay kit (Sangon Biotec, China). The protein was loaded (20 μg per lane), separated by sodium dodecyl sulfate-polyacrylamide gel electrophoresis (SDS-PAGE, Sangon Biotec, China), and then transferred onto polyvinylidene difluoride immobilon-P membrane (PVDF, Millipore). Subsequently, the PVDF membrane was blocked in 5% nonfat milk (Solarbio, China) in TBST (Tris-buffered saline plus 0.1% Tween 20) for an hour, incubated with primary antibodies overnight at 4 °C, and further incubated with the goat antimouse or antirabbit secondary antibody (ProteinTech, China) for an hour at room temperature. After that, the expression of proteins was visualized with an ECL western blotting substrate kit (Sangon Biotech, China), and membranes were photographed using a Tanon 46000SF scanning system.

The primary antibodies GAPDH (ProteinTech, England), Bcl-2 (ProteinTech, England), Bax (Servicebio, China), caspase3 (ProteinTech, England), *c*-caspase3 (ProteinTech, England), γ-H2AX (Ser139, Cell signaling Technology, U.S.A.), P53 (SANTA CRUZ Biotechnology, U.S.A.), MMP9 (ProteinTech, England), COX-2 (ProteinTech, England), *E*-cadherin (Wanleibio, China), *N*-cadherin (Wanleibio, China), vimentin (Wanleibio, China), Snail1 (Wanleibio, China), β-catenin (Wanleibio, China), cyclin D1 (Wanleibio, China), *c*-Myc (Wanleibio, China), and TNF-α (ProteinTech, England) were used.

Immunohistochemical Assay. The expression of proteins in tumor tissues was detected by immunohistochemistry. Tumor tissues of the blank, CDDP, complex **1**, and nanoparticles NPs@CPF_2−Pt(IV) and Tf-NPs@CPF_2−Pt(IV) groups were obtained from the antitumor growth assay in vivo. The tumor tissues were paraffin-embedded and cut with a microtome (5 μm sections). Then, the sections were deparaffinized, hydrated, incubated with the primary antibody overnight at 4 °C, treated with the secondary antibody (Servicebio, China) for 50 min at room temperature, visualized with 3,3′-diaminobenzidine (DAB, Servicebio, China), and counterstained

https://doi.org/10.1021/acs.jmedchem.4c01265
J. Med. Chem. 2024, 67, 16416−16434

using hematoxylin. The primary antibodies COX-2 (Servicebio, China), *E*-cadherin (Servicebio, China), *N*-cadherin (Servicebio, China), *β*-catenin (Servicebio, China), PD-L1 (Servicebio, China), CD3 (Servicebio, China), and CD8 (Servicebio, China) were used. Subsequently, the expression of proteins was imaged with an inverted microscope (Olympus) and measured using ImageJ based on five random visual fields.

Pharmacokinetic Studies. The female SD rats (200−220 g) were randomly assigned to three groups (n = 3). The rats were fasted for 12 h and fed with water before initiating the PK studies. Then, nanoparticles NPs@CPF_2−Pt(IV) and Tf-NPs@CPF_2−Pt(IV), as well as complex **1** injection (dissolved in media of saline containing 5% DMF), were administered intravenously (i.v.) at a dose of 5 mg Pt/kg. Subsequently, blood samples were collected from the retro-orbital plexus at predetermined time points within an 8 h period, and plasma was isolated. The Pt concentration in the plasma was quantified using the AAS assay after digestion with 70% nitric acid (HNO_3) to determine the drug concentration. The PK parameters were calculated with WinNonlin 6.1 software (Pharsight, Inc., Mountain View, CA).

Antitumor Growth Assay In Vivo. The antitumor growth properties were evaluated on BALB/c mice bearing murine 4T1 tumors. Tumor cells (1×10^6 in 0.15 mL PBS) were injected subcutaneously on the left flanks of mice. Then, mice were divided into five groups (n = 6), namely, blank, free complex **1**, nanoparticles NPs@CPF_2−Pt(IV) and Tf-NPs@CPF_2−Pt(IV), and CDDP, when the tumor nodules were palpable on day 4. Complex **1** and CDDP were administrated in saline containing 5% DMF, and the free medium was used in the blank group. The nanoparticles were administrated directly after preparation. The drugs were administrated a same dosage of 2 mg Pt/kg intravenously through the tail vein (i.v.) on days 4, 7, and 10. Then, the mice were sacrificed on day 12, and the blood, tumors, and organs, including the heart, liver, spleen, lung, and kidney, were collected. The tumor volume ($V = W^2 \times L/2$, where W is the width and L is the length of the tumor) and body weight were monitored during the experiment. The weight of tumor tissues was measured after dissection, and the tumor growth inhibition (TGI) was calculated using the following formula: TGI (%) = (1 − tumor weight of the drug-treated group/tumor weight of the blank group) × 100%. The tumor tissues and organs of each group were fixed in 4% paraformaldehyde for 48 h and then dehydrated, embedded in rosin, cut with a microtome (5 μm sections), stained with H&E, and observed under a light microscope. The samples for the ELISA assay were frozen at −80 °C.

Tumor Targeting Studies In Vivo. The DiD with far-red fluorescence was applied as a fluoresce probe to detect the biodistribution of nanoparticles in vivo. Female BALB/c mice bearing murine 4T1 tumors were used for tumor targeting studies in vivo. Tumor cells (1×10^6 in 0.15 mL of PBS) were injected subcutaneously on the left flanks of mice. When the tumor volume reached 200−300 mm^3 on day 7, the mice were randomly divided into three groups (n = 4): the injection of the mixture of DiD with complex **1** (DiD-**1**) and DiD-labeled nanoparticles DiD-NPs@CPF_2−Pt(IV) and DiD-Tf-NPs@CPF_2−Pt(IV). The same volume of drugs with the same concentration of DiD was administrated (i.v.) at the same dosage of 2 mg Pt/kg. The mice were briefly anesthetized by isofluorane inhalation and scanned using an IVIS optical imaging system (Alliance 4.7, UVITEC, Cambridge, U.K.) at 1, 2, 4, 8, 12, and 24 h. After that, the mice were sacrificed. The tissues including the tumor, heart, liver, spleen, lung, and kidney were collected and imaged. The fluorescence intensity in tissues including the tumor, heart, liver, spleen, lung, and kidney was calculated to determine the distribution and the tumor targeting properties of the drugs in vivo with the following formula: relative fluorescence intensity = (fluorescence intensity in specified tissues/fluorescence intensity in all tissues including the tumor, heart, liver, spleen, lung, and kidney) × 100%.

Antimetastatic Assay In Vivo. The antimetastatic assay was performed on female BALB/c mice. The pulmonary metastasis models were established by tail vein injection of 4T1 cells (1×10^5 in 0.2 mL of PBS). Mice were randomly grouped into four groups (n = 5): blank, complex **1**, CDDP, and Tf-NPs@CPF_2−Pt(IV). Complex **1** and CDDP were administrated in media of saline containing 5% DMF, and the free media were used in the blank group. Nanoparticles Tf-NPs@CPF_2−Pt(IV) were administrated directly after preparation. The drugs were administrated at the same dosage of 2 mg Pt/kg (i.v.) on days 3, 6, and 9. Then, the mice were sacrificed on day 12, and the lung tissue was collected and embedded in Bouin's fluid. The number of observable metastasis nodules on the whole surface of the lung was visually counted. The nodules inside the lung were observed after H&E staining with an inverted microscope (Olympus).

Statistical Analysis. Data analysis was performed using Student's t-test or analysis of variance (ANOVA) followed by the q-test with different significance levels ($P < 0.001$, $P < 0.01$, and $P < 0.05$).

■ ASSOCIATED CONTENT

Supporting Information

The Supporting Information is available free of charge at https://pubs.acs.org/doi/10.1021/acs.jmedchem.4c01265.

Synthesis of CPF platinum(IV) complexes; preparation of nanoparticles; reduction of complex **1** in TME; accumulation and distribution of drugs in tumor cells and tissues; mitochondria-mediated apoptosis; DNA damage; antitumor activities in vivo; antimetastatic activities; and ^{1}H NMR, ^{13}C NMR, MS, HRMS, and HPLC spectra of CPF platinum(IV) complexes (PDF)

Molecular formula strings (CSV)

■ AUTHOR INFORMATION

Corresponding Author

Qingpeng Wang − *Institute of Biopharmaceutical Research, Liaocheng University, Liaocheng 252059, P. R. China;* orcid.org/0000-0002-2093-8237; Email: lywqp@126.com

Authors

Ming Zhang − *Institute of Biopharmaceutical Research, Liaocheng University, Liaocheng 252059, P. R. China*

Yan Chen − *Institute of Biopharmaceutical Research, Liaocheng University, Liaocheng 252059, P. R. China; Key Laboratory of Functional Molecular Engineering of Guangdong Province, School of Chemistry and Chemical Engineering, South China University of Technology, Guangzhou 510640, P. R. China*

Shuaiqi Feng − *Institute of Biopharmaceutical Research, Liaocheng University, Liaocheng 252059, P. R. China*

Yanqin He − *Institute of Biopharmaceutical Research, Liaocheng University, Liaocheng 252059, P. R. China*

Zhifang Liu − *Institute of Biopharmaceutical Research, Liaocheng University, Liaocheng 252059, P. R. China*

Ning Zhang − *Institute of Biopharmaceutical Research, Liaocheng University, Liaocheng 252059, P. R. China;* orcid.org/0000-0003-2102-8611

Complete contact information is available at: https://pubs.acs.org/10.1021/acs.jmedchem.4c01265

Notes

The authors declare no competing financial interest.

■ ACKNOWLEDGMENTS

This work was supported by the Youth Innovation Technology Project of Higher School in Shandong Province (No. 2021KJ099), the National Natural Science Foundation of

China (Nos. 21807056 and 22001106), the Natural Science Foundation of Shandong Province (No. ZR2020KH005), and Guangyue Young Scholar Innovation Team of Liaocheng University (No. LCUGYTD2023-03). This work was also technically supported by Shandong Collaborative Innovation Center for Antibody Drugs, Engineering Research Center for Nanomedicine and Drug Delivery Systems, and Taishan Scholar Research Group. The authors thank Home for Researchers, and some figures were drawn by Figdraw.

■ ABBREVIATIONS USED

AAS, atomic absorption spectrometry; AsA, ascorbic acid; CBP, carboplatin; CDDP, cisplatin; COX-2, cyclooxygenase-2; CPF, carprofen; DCFH-DA, 2′,7′-dichlorofluorescein diacetate; DLS, dynamic laser light scattering; DMF, *N,N*-dimethylformamide; DMSO, dimethyl sulfoxide; EMT, epithelial−mesenchymal transition; 5′-GMP, guanosine-5′-monophosphate; H&E, hematoxylin-eosin; HPLC, high-performance liquid chromatography; IC_{50}, half maximal inhibitory concentration; IL, interleukin; i.v., intravenous injection; MMP, matrix metalloproteinase; MTT, 3-(4,5-dimethylthiazol-2-yl)-2,5-diphenyltetrazolium bromide; NDDS, nanodrug delivery systems; NSAIDs, nonsteroidal anti-inflammatory drugs; NPs, nanoparticles; OXP, oxaliplatin; PD-L1, programmed cell death ligand 1; PI, propidium iodide; RF, resistant factor; ROS, reactive oxygen species; SI, selective index; TBTU, *N,N,N′,N′*-tetramethyl-O-(benzotriazol-1-yl)-uronium tetrafluoroborate; TEA, *N,N,N*-triethylamine; Tf, transferrin; TGI, tumor growth inhibition; TILs, tumor-infiltrating lymphocytes; TME, tumor microenvironment; TNF, tumor necrosis factor

■ REFERENCES

(1) Gerstberger, S.; Jiang, Q.; Ganesh, K. Metastasis. *Cell* **2023**, *186* (8), 1564−1579.
(2) Gujral, T. S.; Chan, M.; Peshkin, L.; Sorger, P. K.; Kirschner, M. W.; MacBeath, G. A noncanonical Frizzled2 pathway regulates epithelial-mesenchymal transition and metastasis. *Cell* **2014**, *159* (4), 844−856.
(3) Steeg, P. S. Targeting metastasis. *Nat. Rev. Cancer* **2016**, *16* (4), 201−218.
(4) Zhang, C.; Xu, C.; Gao, X.; Yao, Q. Platinum-based drugs for cancer therapy and anti-tumor strategies. *Theranostics* **2022**, *12* (5), 2115−2132.
(5) Puddephatt, R. J. Supramolecular organometallic chemistry: the platinum(IV) paradigm. *Dalton Trans.* **2022**, *51* (18), 7011−7024.
(6) Tan, X. X.; Li, G. S.; Wang, Q. P.; Wang, B. Q.; Li, D. C.; Wang, P. G. Small molecular platinum(IV) compounds as antitumor agents. *Prog. Chem.* **2018**, *30*, 831−846.
(7) Su, S.; Chen, Y.; Zhang, P.; Ma, R.; Zhang, W.; Liu, J.; Li, T.; Niu, H.; Cao, Y.; Hu, B.; Gao, J.; Sun, H.; Fang, D.; Wang, J.; Wang, P. G.; Xie, S.; Wang, C.; Ma, J. The role of platinum(IV)-based antitumor drugs and the anticancer immune response in medicinal inorganic chemistry. A systematic review from 2017 to 2022. *Eur. J. Med. Chem.* **2022**, *243*, No. 114680.
(8) Chen, Y.; Li, L.; Liu, Z.; Liu, M.; Wang, Q. A series of ligustrazine platinum(IV) complexes with potent anti-proliferative and anti-metastatic properties that exert chemotherapeutic and immunotherapeutic effects. *Dalton Trans.* **2023**, *52* (37), 13097−13109.
(9) Wei, D.; Huang, Y.; Wang, B.; Ma, L.; Karges, J.; Xiao, H. Photoreduction with NIR light of nucleus-targeting PtIV nanoparticles for combined tumor-targeted chemotherapy and photodynamic immunotherapy. *Angew. Chem., Int. Ed.* **2022**, *61* (20), No. e202201486.
(10) Xue, W.; Yang, L.; Chen, C.; Ashrafizadeh, M.; Tian, Y.; Sun, R. Wnt/β-catenin-driven EMT regulation in human cancers. *Cell. Mol. Life Sci.* **2024**, *81* (1), 79.
(11) Fedele, M.; Sgarra, R.; Battista, S.; Cerchia, L.; Manfioletti, G. The epithelial-mesenchymal transition at the crossroads between metabolism and tumor progression. *Int. J. Mol. Sci.* **2022**, *23* (2), 800.
(12) Kang, E.; Seo, J.; Yoon, H.; Cho, S. The post-translational regulation of epithelial-mesenchymal transition-inducing transcription factors in cancer metastasis. *Int. J. Mol. Sci.* **2021**, *22* (7), 3591.
(13) Manfioletti, G.; Fedele, M. Epithelial-mesenchymal transition (EMT) 2021. *Int. J. Mol. Sci.* **2022**, *23* (10), 5848.
(14) Bai, X.; Shao, J.; Duan, T.; Liu, X.; Wang, M.; Li, X.; You, Q.; Zhang, Z.; Pan, J. Exo-miR-1290-induced by COX-2 overexpression promotes cancer-associated fibroblasts activation and tumor progression by CUL3-Nrf2 pathway in lung adenocarcinoma. *Cell Commun. Signal.* **2023**, *21* (1), 242.
(15) Jiang, G. B.; Fang, H. Y.; Tao, D. Y.; Chen, X. P.; Cao, F. L. COX-2 potentiates cisplatin resistance of non-small cell lung cancer cells by promoting EMT in an AKT signaling pathway-dependent manner. *Eur. Rev. Med. Pharmacol. Sci.* **2019**, *23* (9), 3838−3846.
(16) Balamurugan, K.; Poria, D. K.; Sehareen, S. W.; Krishnamurthy, S.; Tang, W.; McKennett, L.; Padmanaban, V.; Czarra, K.; Ewald, A. J.; Ueno, N. T.; Ambs, S.; Sharan, S.; Sterneck, E. Stabilization of *E*-cadherin adhesions by COX-2/GSK3β signaling is a targetable pathway in metastatic breast cancer. *JCI Insight* **2023**, *8* (6), No. e156057.
(17) Sun, C.; Mezzadra, R.; Schumacher, T. N. Regulation and function of the PD-L1 checkpoint. *Immunity* **2018**, *48* (3), 434−452.
(18) Jiang, Y.; Zhan, H. Communication between EMT and PD-L1 signaling: New insights into tumor immune evasion. *Cancer Lett.* **2020**, *468*, 72−81.
(19) Jiang, X.; Wang, J.; Deng, X.; Xiong, F.; Ge, J.; Xiang, B.; Wu, X.; Ma, J.; Zhou, M.; Li, X.; Li, Y.; Li, G.; Xiong, W.; Guo, C.; Zeng, Z. Role of the tumor microenvironment in PD-L1/PD-1-mediated tumor immune escape. *Mol. Cancer* **2019**, *18* (1), 10.
(20) Li, Z.; Wang, Q.; Li, L.; Chen, Y.; Cui, J.; Liu, M.; Zhang, N.; Liu, Z.; Han, J.; Wang, Z. Ketoprofen and loxoprofen platinum(IV) complexes displaying antimetastatic activities by inducing DNA damage, inflammation suppression, and enhanced immune response. *J. Med. Chem.* **2021**, *64* (24), 17920−17935.
(21) Zhang, C. Y.; Guan, X. X.; Song, Z. H.; Jiang, H. L.; Liu, Y. B.; Chen, P.; Duan, J. X.; Zhou, Y. COX-2/sEH dual inhibitor ptupb attenuates epithelial-mesenchymal transformation of alveolar epithelial cells via Nrf2-mediated inhibition of TGF-β1/Smad signaling. *Oxid. Med. Cell Longev.* **2022**, *2022*, No. 5759626.
(22) Buchanan, F. G.; DuBois, R. N. Connecting COX-2 and Wnt in cancer. *Cancer Cell* **2006**, *9* (1), 6−8.
(23) Spector, D.; Krasnovskaya, O.; Pavlov, K.; Erofeev, A.; Gorelkin, P.; Beloglazkina, E.; Majouga, A. Pt(IV) prodrugs with NSAIDs as axial ligands. *Int. J. Mol. Sci.* **2021**, *22* (8), 3817.
(24) Spector, D. V.; Pavlov, K. G.; Akasov, R. A.; Vaneev, A. N.; Erofeev, A. S.; Gorelkin, P. V.; Nikitina, V. N.; Lopatukhina, E. V.; Semkina, A. S.; Vlasova, K. Y.; Skvortsov, D. A.; Roznyatovsky, V. A.; Ul'yanovskiy, N. V.; Pikovskoi, I. I.; Sypalov, S. A.; Garanina, A. S.; Vodopyanov, S. S.; Abakumov, M. A.; Volodina, Y. L.; Markova, A. A.; Petrova, A. S.; Mazur, D. M.; Sakharov, D. A.; Zyk, N. V.; Beloglazkina, E. K.; Majouga, A. G.; Krasnovskaya, O. O. Pt(IV) prodrugs with non-steroidal anti-inflammatory drugs in the axial position. *J. Med. Chem.* **2022**, *65* (12), 8227−8244.
(25) Yu, B.; Wang, Y.; Bing, T.; Tang, Y.; Huang, J.; Xiao, H.; Liu, C.; Yu, Y. Platinum prodrug nanoparticles with COX-2 inhibition amplify pyroptosis for enhanced chemotherapy and immune activation of pancreatic cancer. *Adv. Mater.* **2024**, *36* (11), No. e2310456.
(26) Li, Z.; Li, L.; Zhao, W.; Sun, B.; Liu, Z.; Liu, M.; Han, J.; Wang, Z.; Li, D.; Wang, Q. Development of a series of flurbiprofen and zaltoprofen platinum(IV) complexes with anti-metastasis competence targeting COX-2, PD-L1 and DNA. *Dalton Trans.* **2022**, *51* (33), 12604−12619.

https://doi.org/10.1021/acs.jmedchem.4c01265
J. Med. Chem. 2024, 67, 16416−16434

(27) Chen, Y.; Wang, Q.; Li, Z.; Liu, Z.; Zhao, Y.; Zhang, J.; Liu, M.; Wang, Z.; Li, D.; Han, J. Naproxen platinum(IV) hybrids inhibiting cycloxygenases and matrix metalloproteinases and causing DNA damage: synthesis and biological evaluation as antitumor agents *in vitro* and *in vivo*. *Dalton Trans.* **2020**, *49*, 5192−5204.
(28) Li, L.; Zhang, M.; Jia, D.; Liu, Z.; Zhang, N.; Sun, B.; Wang, Z.; Liu, M.; Wang, Q. Multi-specific niflumic acid platinum(IV) complexes displaying potent antitumor activities by improving immunity and suppressing angiogenesis besides causing DNA damage. *Dalton Trans.* **2022**, *52* (1), 147−158.
(29) Zhang, M.; Chen, Y.; Liu, Z.; Liu, M.; Wang, Q. A series of desloratadine platinum(IV) hybrids displaying potent antimetastatic competence by inhibiting epithelial-mesenchymal transition and arousing immune response. *J. Med. Chem.* **2024**, *67* (3), 2031−2048.
(30) Zhang, M.; Li, L.; Li, S.; Liu, Z.; Zhang, N.; Sun, B.; Wang, Z.; Jia, D.; Liu, M.; Wang, Q. Development of clioquinol platinum(IV) conjugates as autophagy-targeted antimetastatic agents. *J. Med. Chem.* **2023**, *66* (5), 3393−3410.
(31) Li, L.; Chen, Y.; Wang, Q.; Li, Z.; Liu, Z.; Hua, X.; Han, J.; Chang, C.; Wang, Z.; Li, D. Albumin-encapsulated nanoparticles of naproxen platinum(IV) complexes with inflammation inhibitory competence displaying effective antitumor activities *in vitro* and *in vivo*. *Int. J. Nanomed.* **2021**, *Volume 16*, 5513−5529.
(32) Zhang, J.; Wang, S.; Zhang, D.; He, X.; Wang, X.; Han, H.; Qin, Y. Nanoparticle-based drug delivery systems to enhance cancer immunotherapy in solid tumors. *Front. Immunol.* **2023**, *14*, No. 1230893.
(33) Zheng, S.; Li, G.; Shi, J.; Liu, X.; Li, M.; He, Z.; Tian, C.; Kamei, K. I. Emerging platinum(IV) prodrug nanotherapeutics: A new epoch for platinum-based cancer therapy. *J. Controlled Release* **2023**, *361*, 819−846.
(34) Jogadi, W.; Zheng, Y. R. Supramolecular platinum complexes for cancer therapy. *Curr. Opin. Chem. Biol.* **2023**, *73*, No. 102276.
(35) Tang, D.; Zhou, H.; Cui, M.; Liang, G.; Zhang, H.; Xiao, H. NIR-II light accelerated prodrug reduction of Pt(IV)-incorporating pseudo semiconducting polymers for robust degradation and maximized photothermal/chemo-immunotherapy. *Adv. Mater.* **2023**, *35* (28), No. e2300048.
(36) Sancho-Albero, M.; Facchetti, G.; Panini, N.; Meroni, M.; Bello, E.; Rimoldi, I.; Zucchetti, M.; Frapolli, R.; De Cola, L. Enhancing Pt(IV) complexes' anticancer activity upon encapsulation in stimuli-responsive nanocages. *Adv. Healthcare Mater.* **2023**, *12* (17), No. e2202932.
(37) Chan, W. C. W. Principles of nanoparticle delivery to solid tumors. *BME Front.* **2023**, *4*, 0016.
(38) Wei, D.; Fan, J.; Yan, J.; Liu, C.; Cao, J.; Xu, C.; Sun, Y.; Xiao, H. Nuclear-Targeting Lipid Pt^{IV} prodrug amphiphile cooperates with siRNA for enhanced cancer immunochemotherapy by amplifying Pt-DNA adducts and reducing phosphatidylserine exposure. *J. Am. Chem. Soc.* **2024**, *146* (1), 1185−1195.
(39) Wang, W.; Yang, F.; Zhang, L.; Wang, M.; Yin, L.; Dong, X.; Xiao, H.; Xing, N. Targeting DNA damage and repair machinery via delivering WEE1 inhibitor and Platinum (IV) Prodrugs to Stimulate STING pathway for maximizing chemo-immunotherapy in bladder cancer. *Adv. Mater.* **2024**, *36* (1), No. e2308762.
(40) Candelaria, P. V.; Leoh, L. S.; Penichet, M. L.; Daniels-Wells, T. R. Antibodies targeting the transferrin receptor 1 (TfR1) as direct anti-cancer agents. *Front. Immunol.* **2021**, *12*, No. 607692.
(41) Kawak, P.; Sawaftah, N. M. A.; Pitt, W. G.; Husseini, G. A. Transferrin-targeted liposomes in glioblastoma therapy: A review. *Int. J. Mol. Sci.* **2023**, *24* (17), 13262.
(42) Bajracharya, R.; Song, J. G.; Patil, B. R.; Lee, S. H.; Noh, H. M.; Kim, D. H.; Kim, G. L.; Seo, S. H.; Park, J. W.; Jeong, S. H.; Lee, C. H.; Han, H. K. Functional ligands for improving anticancer drug therapy: current status and applications to drug delivery systems. *Drug Delivery* **2022**, *29* (1), 1959−1970.
(43) Mojarad-Jabali, S.; Mahdinloo, S.; Farshbaf, M.; Sarfraz, M.; Fatahi, Y.; Atyabi, F.; Valizadeh, H. Transferrin receptor-mediated liposomal drug delivery: Recent trends in targeted therapy of cancer. *Expert Opin. Drug Delivery* **2022**, *19*, 685−705.
(44) Guan, Q.; Li, Y.; Zhang, H.; Liu, S.; Ding, Z.; Fan, Z.; Wang, Q.; Wang, Z.; Han, J.; Liu, M.; Zhao, Y. Laser-responsive multi-functional nanoparticles for efficient combinational chemo-photo-dynamic therapy against breast cancer. *Colloids Surf. B Biointerfaces* **2022**, *216*, No. 112574.
(45) Lara-Castillo, N.; Kim-Weroha, N. A.; Kamel, M. A.; Javaheri, B.; Ellies, D. L.; Krumlauf, R. E.; Thiagarajan, G.; Johnson, M. L. *In vivo* mechanical loading rapidly activates β-catenin signaling in osteocytes through a prostaglandin mediated mechanism. *Bone* **2015**, *76*, 58−66.
(46) Song, X. Q.; Ma, Z. Y.; Wu, Y. G.; Dai, M. L.; Wang, D. B.; Xu, J. Y.; Liu, Y. New NSAID-Pt(IV) prodrugs to suppress metastasis and invasion of tumor cells and enhance anti-tumor effect *in vitro* and *in vivo*. *Eur. J. Med. Chem.* **2019**, *167*, 377−387.
(47) Xiao, K.; Li, Y.; Luo, J.; Lee, J. S.; Xiao, W.; Gonik, A. M.; Agarwal, R. G.; Lam, K. S. The effect of surface charge on *in vivo* biodistribution of PEG-oligocholic acid based micellar nanoparticles. *Biomaterials* **2011**, *32* (13), 3435−3446.
(48) Ji, F.; Li, J.; Qin, Z.; Yang, B.; Zhang, E.; Dong, D.; Wang, J.; Wen, Y.; Tian, L.; Yao, F. Engineering pectin-based hollow nanocapsules for delivery of anticancer drug. *Carbohydr. Polym.* **2017**, *177*, 86−96.
(49) Zhao, Y.; Zhao, Y.; Ma, Q.; Sun, B.; Wang, Q.; Ding, Z.; Zhang, H.; Chu, X.; Liu, M.; Wang, Z.; Han, J. Carrier-free, dual-functional nanorods via self-assembly of pure drug molecules for synergistic chemo-photodynamic therapy. *Int. J. Nanomedicine* **2019**, *14*, 8665−8683.
(50) Zhang, J.; Wang, L.; Ding, M.; You, X.; Wu, J.; Pang, J. Impact of poly(ester amide) structure on properties and drug delivery for prostate cancer therapy. *BME Front.* **2023**, *4*, 0025.
(51) Liu, N.; Zhou, N.; Chai, N.; Liu, X.; Jiang, H.; Wu, Q.; Li, Q. Helicobacter pylori promotes angiogenesis depending on Wnt/beta-catenin-mediated vascular endothelial growth factor via the cyclo-oxygenase-2 pathway in gastric cancer. *BMC Cancer* **2016**, *16*, 321.
(52) Majumder, M.; Xin, X.; Liu, L.; Tutunea-Fatan, E.; Rodriguez-Torres, M.; Vincent, K.; Postovit, L. M.; Hess, D.; Lala, P. K. COX-2 Induces Breast Cancer Stem Cells via EP4/PI3K/AKT/NOTCH/WNT Axis. *Stem Cells* **2016**, *34* (9), 2290−2305.
(53) Katoh, M. Multi-layered prevention and treatment of chronic inflammation, organ fibrosis and cancer associated with canonical WNT/β-catenin signaling activation (Review). *Int. J. Mol. Med.* **2018**, *42* (2), 713−725.
(54) Hanahan, D. Hallmarks of cancer: New dimensions. *Cancer Discovery* **2022**, *12* (1), 31−46.
(55) Kalyane, D.; Raval, N.; Maheshwari, R.; Tambe, V.; Kalia, K.; Tekade, R. K. Employment of enhanced permeability and retention effect (EPR): nanoparticle-based precision tools for targeting of therapeutic and diagnostic agent in cancer. *Mater. Sci. Eng. C Mater. Biol. Appl.* **2019**, *98*, 1252−1276.

https://doi.org/10.1021/acs.jmedchem.4c01265
J. Med. Chem. 2024, 67, 16416−16434